Isotopic fractionation of nitrous oxide in the stratosphere: Comparison between model and observations

C. G. Morgan,[1] M. Allen,[2] M. C. Liang, R. L. Shia, G. A. Blake, and Y. L. Yung
Division of Geological and Planetary Sciences, California Institute of Technology, Pasadena, California, USA

Received 10 January 2003; revised 17 September 2003; accepted 2 October 2003; published 20 February 2004.

[1] We investigate the mass dependent isotopic fractionation mechanisms, based on photolytic destruction and reaction with $O(^1D)$, to explain the $^{15}N/^{14}N$ and $^{18}O/^{16}O$ fractionation of stratospheric N_2O and reconcile laboratory experiments with atmospheric observations. The Caltech/JPL two-dimensional (2-D) model is utilized for detailed studies of N_2O and its isotopologues and isotopomers in the stratosphere. We compare model results with observations of isotopic enrichment using three different methods of calculating photolytic cross-sections for each of the major isotopologues and isotopomers of N_2O. Although the *Yung and Miller* [1997] successfully modeled the pattern of enrichments for each isotopologue or isotopomer relative to each other, their approach underestimated the magnitude of the enrichments. The ab initio approach by *Johnson et al.* [2001] provides a better fit to the magnitudes of the enrichments, with the notable exception of the enrichment for the $^{15}N^{14}N^{16}O$. A simpler, semi-empirical approach by *Blake et al.* [2003] is able to model the magnitude of all the enrichments, including the one for $^{15}N^{14}N^{16}O$. The *Blake et al.* [2003] cross-sections are temperature-dependent, but adjustments are needed to match the measurements of *Kaiser et al.* [2002a]. Using these modified cross-sections generally improves the agreement between model and mass spectrometric measurements. Destruction of N_2O by reaction with $O(^1D)$ results in a small but nonnegligible isotopic fractionation in the lower stratosphere. On a per molecule basis, the rates of destruction of the minor isotopologues or isotopomers are somewhat less than that for $^{14}N^{14}N^{16}O$. From our 2-D model we infer the relative rates for isotopologues and isotopomers $^{14}N^{14}N^{16}O$ (446), $^{14}N^{15}N^{16}O$ (456), $^{15}N^{14}N^{16}O$ (546), $^{14}N^{14}N^{17}O$ (447) and $^{14}N^{14}N^{18}O$ (448), to be 1, 0.9843, 0.9942, 0.9949, and 0.9900, respectively. Thus the destruction of N_2O in the atmosphere results in isotopic fractionations of (456), (546), (447) and (448) by 19.4, 9.5, 5.5 and 12.0‰. If we do not distinguish between the (456) and (546) isotopomers, the mean isotopic fractionation for ^{15}N is 14.5‰. If we assume that the mean tropospheric values for δ_{456}, δ_{546}, $\delta^{15}N$ and $\delta^{18}O$ are 16.35, −2.35, 7.0 and 20.7‰, respectively, we infer the following isotopic signature for the integrated sources of N_2O: $\delta_{456} = -2.9$‰, $\delta_{546} = -11.7$‰, $\delta^{15}N = -7.3$‰ and $\delta^{18}O = 8.7$‰. *INDEX TERMS:* 0315 Atmospheric Composition and Structure: Biosphere/atmosphere interactions; 0341 Atmospheric Composition and Structure: Middle atmosphere—constituent transport and chemistry (3334); 1040 Geochemistry: Isotopic composition/chemistry; 1610 Global Change: Atmosphere (0315, 0325); 1615 Global Change: Biogeochemical processes (4805); *KEYWORDS:* isotope, N_2O, stratosphere

Citation: Morgan, C. G., M. Allen, M. C. Liang, R. L. Shia, G. A. Blake, and Y. L. Yung (2004), Isotopic fractionation of nitrous oxide in the stratosphere: Comparison between model and observations, *J. Geophys. Res.*, *109*, D04305, doi:10.1029/2003JD003402.

1. Introduction

[2] The present terrestrial atmosphere contains about 310 ppbv (1 part per billion by volume = 1 nmol mol^{-1} [*Prinn et al.*, 2000]) of nitrous oxide (N_2O). N_2O is produced mainly by microbes as a part of the nitrogen cycle [*Stein and Yung*, 2003]. It is removed from the atmosphere primarily by photodissociation

$$N_2O + h\nu \rightarrow N_2 + O(^1D) \quad (1)$$

with a smaller loss (∼10%) from the photo-oxidation reaction with $O(^1D)$

$$N_2O + O(^1D) \rightarrow 2\,NO \quad (2a)$$

$$\rightarrow N_2 + O_2 \quad (2b)$$

[1]Now at SRI International Molecular Physics Laboratory, Menlo Park, California, USA.

[2]Also at Earth and Space Sciences Division, Jet Propulsion Laboratory, California Institute of Technology, Pasadena, California, USA.

0148-0227/04/2003JD003402

It is convenient to summarize the rate of destruction of N_2O as a linear process $L\chi$, where χ is the mixing ratio of N_2O, and L is the loss coefficient due to the above processes

$$L = J_1 + (k_{2a} + k_{2b})\left[O(^1D)\right] \quad (3)$$

where J_1 is the photodissociation rate constant for reaction (1) and k_{2a} and k_{2b} are the rate constants for reactions (2a) and (2b). Both reactions (1) and (2) take place primarily in the stratosphere, resulting in a mean lifetime of about 120 years for N_2O [*Minschwaner et al.*, 1993; *Olsen et al.*, 2001]. Reaction (2a) is the major source of odd nitrogen (NO_x) to the stratosphere and plays a fundamental role in regulating the ozone layer [see, e.g., *Logan et al.*, 1978; *Wennberg et al.*, 1994].

[3] On a per molecule basis, N_2O is about 206 times as effective as CO_2 in causing global warming in the present atmosphere [*Houghton et al.*, 1990]. A doubling of atmospheric N_2O would cause the mean global surface temperature to increase by 0.7°C [*Wang et al.*, 1976; *Houghton et al.*, 1990, 2001], which is approximately the total observed mean global warming in the last hundred years. An increase in atmospheric N_2O was predicted to occur in connection with enhanced agricultural activity [*McElroy et al.*, 1977]. However, there was disagreement on the projected rate of increase of N_2O [see, e.g., *Yung et al.*, 1976]. The actual rate of increase has been determined by high precision gas chromatography measurements of atmospheric flask samples. The data suggest that the rate of N_2O increase was about 0.5–0.6 ppbv yr^{-1} during 1976–82, increased to 0.8–1 ppbv yr^{-1} in 1988–90, and returned to a rate of 0.5–0.6 ppbv yr^{-1} in recent years [*Weiss*, 1981; *Zander et al.*, 1994; *Khalil and Rasmussen*, 1995]. In addition, it has been found that during the last ice age (18,000 years ago), the atmosphere contained only 200 ppbv of N_2O [*Leuenberger and Siegenthaler*, 1992; *Flückiger et al.*, 1999], as compared to the preindustrial value of 280 ppbv. The present N_2O concentration in the atmosphere is 55 and 11% above the ice age and preindustrial values, respectively. While the increase of N_2O from the ice age to the preindustrial level was clearly part of the natural climate/biosphere cycle, the increase from the preindustrial to the present level was most likely caused by human activities. The historical increase of N_2O is likely to continue into the future.

[4] The continued increase of N_2O in the atmosphere is a serious environmental concern for the reasons stated above. As a consequence, N_2O is one of the gases targeted for regulation by the Kyoto Protocol (available at http://www.iisd.ca/climate/kyoto), the other gases being CO_2, CH_4, SF_6, hydrofluorocarbons and perfluorocarbons. According to a recent analysis [*Nevison and Holland*, 1997], the current increase rate, 0.6–1 ppbv yr^{-1}, or 0.2–0.3% per year, represents an excess of 30–50% of global emissions over current sinks. Therefore to stabilize concentrations at the present level, an immediate reduction of 70–80% of the additional flux of N_2O that has occurred since the industrial revolution would be necessary. Without immediate steps taken to regulate N_2O emissions, the atmospheric concentration is expected to rise to 400–500 ppbv, or about twice the preindustrial concentration. However, the N_2O budget is at present not well quantified, making it difficult to determine the sources and the cause of its increase precisely [*Houghton et al.*, 1996; *Cicerone*, 1989; *Khalil and Rasmussen*, 1992]. *Houghton et al.* [2001, Table 4.4] summarizes the current knowledge of the budget of N_2O. The range of uncertainty is quite large, exceeding a factor of two in many cases. This is obviously an unsatisfactory state of knowledge for a gas that we wish to regulate. We shall argue that an understanding of the isotopes of N_2O is the key to a better budget of the sources of N_2O.

[5] A most powerful method for characterizing the sources of N_2O lies in its multi-isotope signature, as demonstrated in the seminal work by *Kim and Craig* [1993] (hereafter referred to as KC93). (*Kaiser et al.* [2002a] pointed out the largely ignored preKC93 work on isotopic fractionation.) The significant results of KC93 are: (1) the major land biospheric sources of N_2O are light in both ^{15}N and ^{18}O, relative to tropospheric N_2O, (2) stratospheric N_2O is heavy in both ^{15}N and ^{18}O, relative to tropospheric N_2O, and (3) there must be a large "back flux" of heavy N_2O from the stratosphere to the troposphere in order to account for the isotopic composition of tropospheric N_2O. Therefore if we could compute (4) in an atmospheric model, we would have a constraint on the isotopic composition of the biological source.

[6] This paper is focused on the isotopic fractionation of N_2O in the stratosphere and its implications for the budget of N_2O. Following a discussion of the mechanisms and observations, we use the Caltech/JPL two-dimensional (2-D) model to simulate the observed isotopic fractionations of N_2O in the stratosphere. A tentative budget for the isotopic source from the biosphere is deduced from this study. This work complements a recent study of the same subject with emphasis on the ^{18}O anomaly using a 3-D model [*McLinden et al.*, 2003].

2. Isotopic Fractionation of N_2O: Mechanisms and Observations

[7] There are three important isotopologues of N_2O: ^{15}NNO, $N_2{}^{18}O$ and $N_2{}^{17}O$. In addition, there are two ^{15}N isotopomers of N_2O: ^{15}NNO and $N^{15}NO$. For definitions of "isotopologue" and "isotopomer", the reader is referred to the International Union of Pure and Applied Chemistry (IUPAC) Compendium of Chemical Terminology 2nd Edition [1997]. Hereafter, we will refer to $^{14}N^{14}N^{16}O$, $^{14}N^{15}N^{16}O$, $^{15}N^{14}N^{16}O$, $^{14}N^{14}N^{17}O$, and $^{14}N^{14}N^{18}O$ as (446), (456), (546), (447) and (448), respectively. $N^{\alpha}NO$ (N^2NO) and $^{\beta}NNO$ (^1NNO) are also used in the literature to denote the central and terminal positions of the N atom in N_2O, respectively. See *Kaiser et al.* [2002a, Appendix] for a detailed discussion.

[8] For the isotopic fractionation of isotopologues and isotopomers of N_2O, it is convenient to adopt the δ notation, defined as follows:

$$\delta_i(‰) = \left(\frac{R_i}{R_{std}} - 1\right) \times 1000 \quad (4)$$

where $R_i = (^{15}N/^{14}N)$, $(^{17}O/^{16}O)$ or $(^{18}O/^{16}O)$ in the sample of interest, and R_{std} is same ratio in a standard sample [*O'Neil*, 1986]. For the purposes of this study, the values of R_{std}, based on elemental abundances, are 0.003690, 0.003690, 0.0003729 and 0.002039 for (456), (546), (447) and (448), respectively. As the destruction of N_2O is characterized by a

linear loss mechanism, the fractionation of isotopically substituted N_2O can be considered a Rayleigh fractionation process, which is described by the following ratio:

$$\frac{(\delta_i + 1)}{(\delta_{0,i} + 1)} = f^{\varepsilon_i} \quad (5)$$

In Equation (5), δ_i is the delta value for isotopologue or isotopomer i, while $\delta_{0,i}$ is the delta value in the troposphere. The quantity f is the fraction of N_2O remaining in the parcel of air and ϵ_i is the measured rate of fractionation, also known as the enrichment, for isotopologue or isotopomer i in the stratosphere. Taking logarithms of both sides, we have

$$\ln[(1 + \delta_i)/(1 + \delta_{0i})] = \varepsilon_i \ln f \quad (6)$$

If we make the approximation that $\ln(1 + \delta) \approx \delta$ for $\delta \ll 1$, a linear relationship between f and δ_i can be derived, $\delta_i \approx \delta_{0,i} + \varepsilon_i \ln f$, where ε_i is the slope of the line. However, this is a poor approximation for N_2O studies [see *Kaiser et al.*, 2002a, Appendix]. For example, for $\delta_i = 100‰$, $\ln(1 + \delta_i) = 95.3‰$ and the difference between the two is 4.7‰, an unacceptably large error. Unless otherwise stated, we will use (6) in this paper. The enrichment ε_i [see, e.g., *Toyoda et al.*, 2001] is not the same as the fractionation constant [see, e.g., *Kaiser et al.*, 2002a; *McLinden et al.*, 2003], except in a limiting case. For a detailed relation in a 1-D model, see equations (B27–B28) in appendix B. There should be no confusion because the context in which they are used is different.

[9] Following the discovery of the N_2O isotopic anomaly by KC93; *Johnston et al.* [1995] attempted to verify the suggestion that stratospheric chemistry results in N_2O isotopic fractionation. However, laboratory experiments measured very little isotopic enrichment in photolyzed or photo-oxidized $N_2{}^{16}O/N_2{}^{17}O/N_2{}^{18}O$ samples. These studies and the possibility of an unidentified reaction in the stratosphere have led to several proposals for new sources of N_2O in the upper atmosphere [*McElroy and Jones*, 1996; *Prasad*, 1994, 1997, 1998; *Zipf and Prasad*, 1998]. *Yung and Miller* [1997] (hereafter referred to as YM97) pointed out that the photodissociation experiments of *Johnston et al.* [1995] did not provide a definitive test of photolysis as a mechanism for fractionation because these experiments were performed at 185 nm [see also *Kaiser et al.*, 2003], sampling a portion of the absorption spectrum near the cross-section maximum. Here the value of the cross-section is particularly insensitive to a spectral shift caused by isotopic substitution of the N_2O molecule. The bulk of atmospheric N_2O photodestruction occurs around 200–202 nm due to the convolution of the N_2O absorption cross-sections with the atmospheric UV transmission window [*Minschwaner et al.*, 1993]. Mindful of this, YM97 proposed a wavelength-dependent mechanism for the photolytic fractionation of N_2O based on subtle shifts in the zero point energies (ZPE) with isotopic substitution. For example, substituting ^{18}O for ^{16}O results in a calculated ZPE blue shift for the heavier isotopologue of $-27.5\ cm^{-1}$. While the cross-sections are essentially identical at the absorption peak, a clear separation is manifest on both shoulders. Analogous to the kinetic fractionation for a chemical reaction, the photolysis fractionation factor will be equal to the ratio of the heavy-to-light photolysis rates and thus to the ratio of the cross-sections. For N_2O, the theoretical fractionation can be calculated analytically as a function of wavelength using the spectral function of *Selwyn et al.* [1977], and the YM97 model was able to match, at least qualitatively, the observed enrichments of both ^{15}N and ^{18}O.

Table 1. Isotopic Fractionation of N_2O–Stratospheric Observations

Reference	Latitude(s)	Month(s)	Method[a]	Range of ln f
Rahn and Wahlen [1997]	45°N	January, April, May	MS	0–(−0.8)
	65°N	February		
Griffith et al. [2000]	35°N	May, September	FTS	(−0.3)–(−2.3)
	65°N	March, May, July, December		
Röckmann et al. [2001]	15°N	April	MS	0.0–(−0.6) (lower)
	45°N	September		(−0.6)–(−4.0) (upper)
	65°N	January–March		
Toyoda et al. [2001]	35°N	May	MS	0.0–(−0.6) (lower) (−0.6)–(−4.0) (upper)

[a]MS, Mass Spectrometer; FTS, Fourier Transform Spectrometer.

[10] Photolysis experiments investigating the validity of the YM97 theory were performed by *Rahn et al.* [1998], *Röckmann et al.* [2000], *Turatti et al.* [2000], and *Zhang et al.* [2000]. The data are clearly consistent with a simple Rayleigh fractionation model, and the trend of the heavy isotope enrichment with wavelength were consistent with that predicted by YM97. It was observed that enrichments of ^{15}N to ^{18}O yields ratios that were slightly greater than unity at wavelengths close to the effective or mean stratospheric photolysis wavelength of 205 nm. This is nearly identical to the ratio of the enrichments observed in *Rahn and Wahlen* [1997] and close to that predicted in Figure 2 of YM97; it supports the hypothesis that photolysis is the principal mechanism responsible for the observed stratospheric enrichments and that the standard model of stratospheric N_2O chemistry is essentially complete. *Turatti et al.* [2000] and *Zhang et al.* [2000] observed that the enrichment for the $^{14}N^{15}N^{16}O$ was greater than that for the isotopomer $^{15}N^{14}N^{16}O$, as predicted by YM97. The magnitudes of the experimentally determined enrichments were all found to be much greater than that predicted by YM97, however. For example, the ^{18}O enrichment at 207.6 nm was found to be −46.0 ‰, more than twice that predicted by YM97.

[11] Several papers have reported observations of N_2O isotopic fractionation in the stratosphere. Information about these measurements is presented in Table 1. *Griffith et al.* [2000] (Griffith et al., manuscript with revisions, 2003; Griffith, private communication, 2003) analyzed Fourier Transform Spectrometer (FTS) data collected through limb sounding on a balloon platform, while *Rahn and Wahlen* [1997], *Röckmann et al.* [2001] and *Toyoda et al.* [2001] report on direct stratospheric sampling followed by analysis using a mass spectrometer. The two latter mass spectrometer studies were able to differentiate between the $^{14}N^{15}N^{16}O$ and $^{15}N^{14}N^{16}O$ isotopomers by examining the $^{14}N^{16}O$ and $^{15}N^{16}O$ fragments. The results of these observations are consistent with the laboratory results; while the pattern of isotopic enrichment between isotopologues and isotopomers is predicted by YM97, the magnitude of these effects is

greater in the observations than what is predicted by theory. For example, the ^{18}O stratospheric enrichment of *Toyoda et al.* [2001] was found to be −24.6‰; YM97 predicts an enrichment of −13.2‰. The enrichment values deduced from the FTS measurements were about 55–80% higher than those of the mass spectroscopic (MS) measurements, and the errors associated with the FTS enrichment were between 17 and 70%.

[12] Theoretical modeling to extend photodestruction induced isotopic fractionation to include other aspects of photolysis was carried out by *Johnson et al.* [2001] and *Blake et al.* [2003]. A full description of the approach used by *Johnson et al.* [2001] can be found in their paper. The factors included in their theoretical description of heavy isotopologue or isotopomer enrichment by photolysis are (1) ZPE shift, (2) excited-state potential energy surfaces, (3) bending mode excitation in the ground electronic state, (4) the transition dipole surface, and (5) the initial wave function. The net effect of these factors is that the magnitude of the isotopologue and isotopomer enrichment is greater than that calculated by YM97. Since the emphasis of *Johnson et al.* [2001] was on deriving the photolytically-driven enrichment and not on reproducing the N_2O ultraviolet absorption curve, there is about a 3 nm difference between the theoretical absorption profile reported and the standard absorption curve that NASA recommends [*DeMore et al.*, 1997]. In order not to avoid spurious effects due to differences between the theoretical and standard absorption curves, the theoretical absorption profiles were renormalized with respect to the standard profiles of *DeMore et al.* [1997].

[13] The approach of *Blake et al.* [2003] is to describe the changes to the absorption profile with a pseudo-diatomic molecule Born-Oppenheimer model. Further details of the theory will be presented in a paper by M. C. Liang et al. (A semi-analytic model for photo-induced isotopic fractionation in simple molecules, manuscript submitted to Journal of Geophysical Research, 2003), but we review the salient details here. This method takes advantage of the fact that we are not interested in the absolute value of the absorption profile for each isotopologue or isotopomer but rather in the small changes between the main isotopologue and the others. In the Born-Oppenheimer limit, the electronic ground state and excited potential energy surfaces are independent of isotopic substitution. However, the vibrational wave functions are affected with changes in geometry leading to shifts in the absorption cross-sections (similar to that envisioned in YM97) and changes in eigenstate energy (the ZPE shifts) leading to changes in the shape of the absorption cross-sections. If the vibrations are treated as slightly anharmonic oscillators, the absorption cross-sections may be fit as the product of an isotopically-independent polynomial of order five with an isotopologue-specific Gaussian function. The polynomial function accounts for the curvature of the electronically excited potential energy surface and the variation of the dipole matrix element with geometry, and the results of such a fit to the $^{14}N^{14}N^{16}O$ are shown in Figure 1a. The sharp structure in the cross-section above energies of 50,000 cm^{-1} arises from absorption out of excited bending states of nitrous oxide. Provided the vibrational frequencies of all the isotopologues and isotopomers are known, their cross-sections can be accurately calculated using only experimental data. In all systems investigated to date (the hydrogen halides, water, ozone, and nitrous oxide), the ZPE-induced shape changes dominate over the cross-section shifts, resulting in a fractionation pattern that is strongly curved with frequency.

[14] For N_2O, the excited electronic state has a nonlinear minimum, which leads to poor Franck-Condon overlap with the vibrational ground state. The total absorption profile is therefore fit as a temperature dependent sum of three Gaussians corresponding to the absorption profile of the ground vibrational state and the first two excited bending states. The parameters associated with each profile were found using measurements over a range of temperatures. The standard N_2O absorption profiles were done using data measured with wavelengths less than 200 nm. Including the measurements of *Yoshino et al.* [1984] and *Mérienne et al.* [1990] insures that data associated with the wavelength region of photolysis critical to the stratosphere (∼201 nm) is used in the parameterization.

[15] A comparison between the three cross-section models and laboratory data is shown in Figure 1b. The laboratory measurements are taken from *Rahn et al.* [1998], *Röckmann et al.* [2000, 2001], *Turatti et al.* [2000], *Zhang et al.* [2000], data reanalyzed by D. Griffith, 2001, Griffith, private communication, 2003, and *Kaiser et al.* [2002b]. The data are represented in Figure 1b as a plot of $(\sigma_i/\sigma_{446} - 1)$ versus photolysis wavelength, where σ_i and σ_{446} are photodissociation cross-sections for isotopologue or isotopomer (i) and (446), respectively. In general, the semi-empirical model of *Blake et al.* [2003] predicts more fractionation than the other two models. As discussed in their paper, the ZPE model of YM97, which is the straight dotted line on the graphs, lacks the curvature needed to match the data, since it only considers one of the factors leading to isotopic fractionation by photolysis. If the fractionation curves for each of the isotopologues are examined in detail, it can be seen that the pseudo-diatomic model of *Blake et al.* [2003] provides a better match for the laboratory data of the ^{15}N substituted isotopologues and isotopomers of N_2O than the other two models. In particular, the semi-empirical model does not have the 205 nm "hump" in the (546) isotopomer enrichment curve predicted by the ab initio model (dashed line in Figure 1b) of *Johnson et al.* [2001]. The most likely cause of the discrepancy is the assumption that the N-N bond length is fixed [*McLinden et al.*, 2003]. The Born-Oppenheimer model also provides as good a match to the ^{18}O substituted isotopologue of N_2O as the ab initio model.

[16] Recently, *Kaiser et al.* [2002a] measured the fractionation factors for N_2O from 193 to 295 K at 207 nm. The temperature-dependent cross-sections for (448), (456), and (546) have been computed by *Blake et al.* [2003] at all wavelengths and temperatures relevant to the stratosphere. A detailed comparison between *Kaiser et al.* [2002a] and *Blake et al.* [2003] will be given in *Liang et al.*, [2003, manuscript in preparation, 2003]. (456) is in good agreement with the measurements, with difference <5‰. However, the model values for (448) and (546) differ significantly from that of the laboratory measurements, about 5‰ at room temperature and reaching 10–15‰ at 210 K. In order to test the impact of *Kaiser et al*'s [2002a] measurements in our model, we modified the cross-sections of *Blake et al.* [2003] to match the 207 nm measurements. The temperature-dependent adjustment factors are then

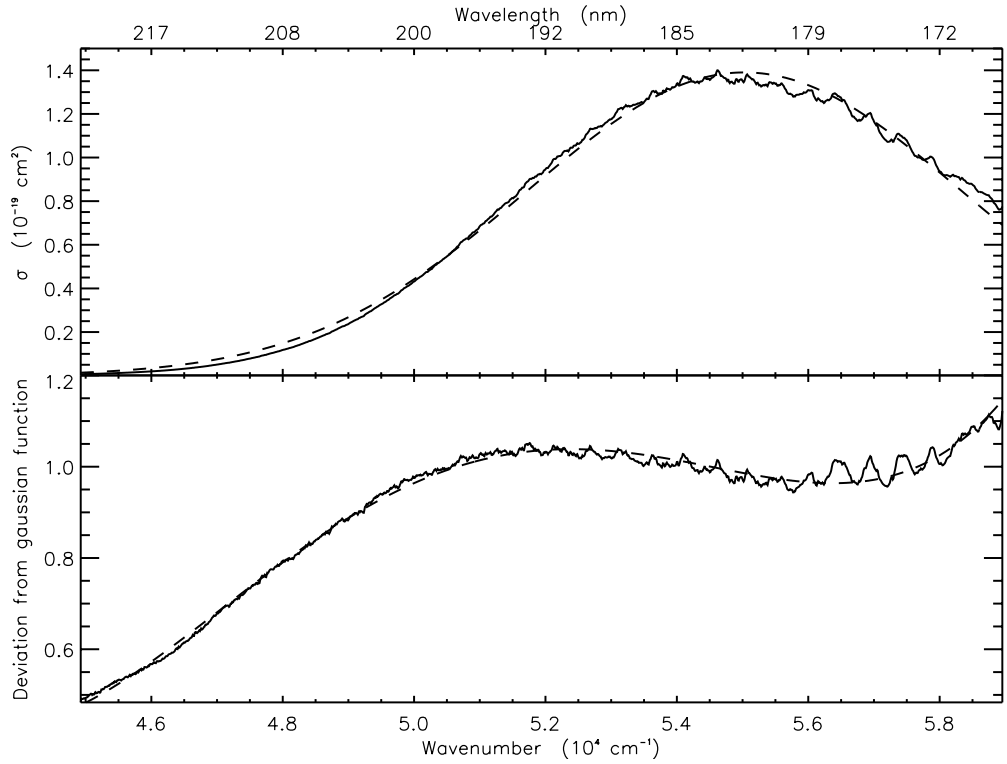

Figure 1a. (top) A gaussian best fit (dashed line) to the room temperature laboratory $^{14}N^{14}N^{16}O$ cross-section data of *Yoshino et al.* [1984] (solid line). (bottom) A fifth order isotopologue-independent polynomial (dashed line) that accounts for factors such as the variation of the dipole matrix element with geometry and the curvature in the excited state potential energy surface. This curve is obtained by taking the ratio between the measured cross-section and the fitted gaussian curve.

uniformly applied to the whole wavelength region. We do not have temperature-dependent measurements of the cross-sections for (447). The adjustment is scaled from (448). The net result is that the modified *Blake et al.* [2003] cross-sections are within 1‰ of the original cross-sections.

[17] *Kaiser et al.* [2002b] reported measurements of N_2O fractionation in its reaction with $O(^1D)$ atoms. Their room temperature data show enrichment of -8.79‰ for (546), -2.22‰ for (456) and -12.23‰ for (448). Although this channel for N_2O loss is very small over the entire stratosphere, in the lower parts of the stratosphere its contribution can be significant. The authors suggest that fractionation from this channel might explain the fact that the observed ratio of enrichment of $^{14}N^{15}N^{16}O$ over enrichment of $^{15}N^{14}N^{16}O$ is smaller than would be expected if only photolysis and transport influenced fractionation.

3. Two-Dimensional Chemical Transport Model

[18] We use the Caltech/JPL 2-D model for simulating the distribution of N_2O in the atmosphere. The continuity equation

$$\frac{\partial \chi}{\partial t} + \nu \frac{\partial \chi}{\partial y} + w \frac{\partial \chi}{\partial z} - \frac{1}{\cos\theta} \frac{\partial}{\partial y}\left\{\cos\theta K_{yy} \frac{\partial \chi}{\partial y}\right\} - e^{\xi} \frac{\partial}{\partial z}\left\{e^{-\xi} K_{zz} \frac{\partial \chi}{\partial z}\right\} = \frac{Q}{M} \quad (7)$$

is solved for all important, long-lived species where χ is the mixing ratio for the species. The details of the model are in appendix A. The model uses NASA recommendations for stratospheric modeling of the rate constants of the gas phase reactions [*DeMore et al.*, 1997]. The chemical destruction reactions of N_2O, listed in Equations (1) and (2), are discussed in the Introduction. For completeness, the production channel of N_2O

$$N_2 + O(^1D) + M \rightarrow N_2O + M \quad (8)$$

is also included. The model is run for 13 years, during which climatological and radiation updates to the model are done monthly. A standard mixing ratio of 3.1×10^{-7} for N_2O is used to start the run. For the minor isotopologues and isotopomers, the initial concentrations and the rates of N_2O production are calculated using the standard isotopic ratios. For all the runs, only the concentrations of N_2O and $O(^1D)$ are allowed to vary. Concentrations of ozone are fixed using the climatology recommended by the SPARC [*Fortuin and Kelder*, 1998; *Randel and Wu*, 1999]. The model is run with each set of photolytic cross-sections discussed earlier. In a second set of runs, the fractionation effects of the destruction rates of N_2O by $O(^1D)$ are added to the model. The second set of runs will be our standard case for the rest of the paper.

4. Results and Discussions

4.1. The Most Abundant Isotopologue $^{14}N^{14}N^{16}O$

[19] A first test of the validity of our model is a comparison of the mixing ratio of N_2O predicted by the model with

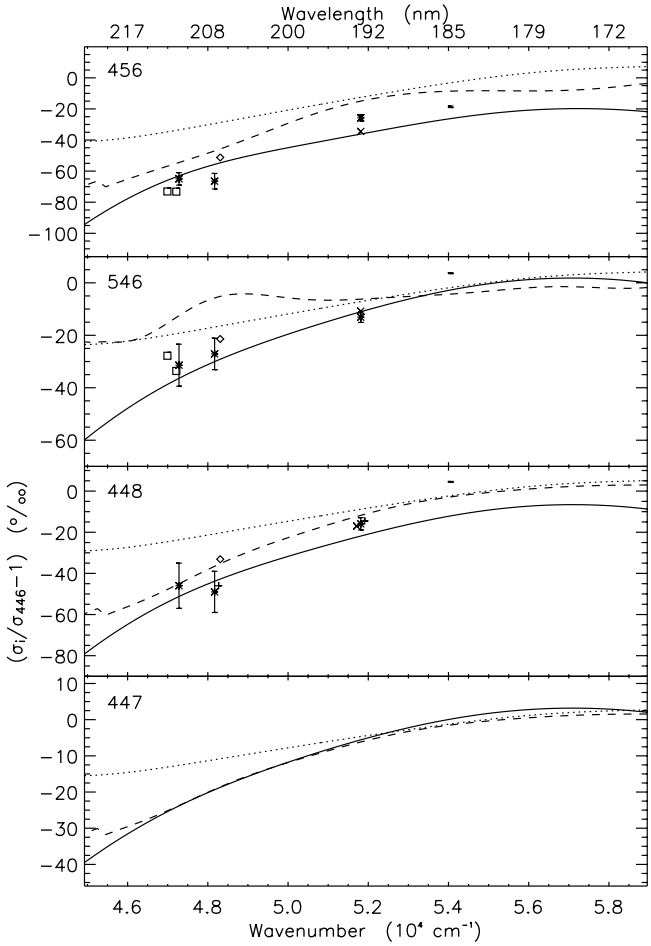

Figure 1b. A summary of the various theoretical fractionation models (this work, solid line; *Yung and Miller* [1997], dotted line; *Johnson et al.* [2001], dashed line) superimposed on room temperature laboratory mass spectrometric (*Rahn et al.* [1998], plusses; *Röckmann et al.* [2000], crosses; *Röckmann et al.* [2001], diamonds; *Kaiser et al.* [2002], closed squares) and infrared spectroscopic measurements (*Turatti et al.* [2000], asterisks; *Zhang et al.* [2000], open squares) of nitrous oxide photolysis. The corresponding error bars for the measurements are overplotted only for those with error bars greater than their symbol size. The error bars are 2σ.

observations. For this purpose we use the results of the Atmospheric Trace Molecule Spectroscopy Experiment (ATMOS) campaigns [*Gunson et al.*, 1990; *Nightingale et al.*, 1993]. These profiles have been observed in almost all latitudinal bands for the months of March, April and November. Concentration profiles of N_2O were binned into 10° latitudinal bands for each month. An example of the comparison between observations and the model at 15 N for March can be seen in Figure 2 and reveals fairly good agreement. We also give the mixing ratio of N_2O on the ln f scale in this figure. In the troposphere, where there is negligible loss of N_2O, ln f is close to 0. For later reference, it is convenient to divide the stratosphere roughly into two regions: the lower stratosphere where ln $f > -0.6$, and the upper stratosphere where ln $f < -0.6$. There is an area of noticable discrepancy between the model and observation at very high altitudes (<1 mbar pressure). However, there is great uncertainty in the measurements in this region, and the discrepancy does not imply model deficiencies. The model 2-D mixing ratios are generally in agreement with previous studies [e.g., *Proffitt et al.*, 1992].

4.2. Isotopic Fractionation in the Stratosphere

[20] The second test of the validity of the model is the comparison between calculated enrichment values and those observed in the stratosphere. For our model, f is calculated relative to a standard mixing ratio for N_2O of 3.1×10^{-7} at the surface. The contribution by radiation to the fractionation factor for isotopologue or isotopomer (i) is given by $(\alpha_i - 1)$, where α_i is the ratio between J_i and J_{446}. Figure 3a shows a plot of $(\alpha_i - 1)$ versus ln f for the model using the cross-sections computed by *Blake et al.* [2003]. These data were from May at 35°N, corresponding to the observations of *Toyoda et al.* [2001]. This plot shows that the contribution by radiation to fractionation is fairly constant over a large range of N_2O concentration. Figure 3b shows a plot of $\ln(1 + \delta)$ versus ln f for the model using the same cross-sections at the same latitude and month. In this plot there are two domains of linearity, each with different slopes. The first domain corresponds to the lower stratosphere below roughly 27 km, where ln f ranges from −0.04 to −0.6. The second corresponds to the upper stratosphere between roughly 27 and 50 km; the ln f for this domain ranges from −0.6 to −4.0. These domains of linearity in the model are also present in the observations of *Röckmann et al.* [2001] and *Toyoda et al.* [2001].

[21] For each isotopologue or isotopomer, the enrichment ϵ_i can be determined by calculating a least squares fit either to the model data or to the observations. Model results are averaged over the time periods and latitude bands corresponding to the observations and reported in Table 1. They are also averaged over the last five years of the model run, the period of time when the model should reach steady state. An example of the least squares fit is shown in Figure 4. For the upper stratospheric region, the enrichment values derived from the model run, for each isotopologue and isotopomer and the average of the ^{15}N isotopomers, are shown in Table 2, along with the observed values of *Griffith et al.* [2000] (and Griffith et al. update, 2003; Griffith, private communication, 2003), *Röckmann et al.* [2000], and *Toyoda et al.* [2001]. A comparison between the model enrichment, without including the $O(^1D)$ fractionation channel, and observations for the lower stratosphere is shown in Table 3. Additionally, Table 4 shows the lower stratospheric measurements including fractionation by the $O(^1D)$ loss reaction of N_2O. Since the data for *Rahn and Wahlen* [1997], *Griffith et al.* [2000] and *Röckmann et al.* [2000] were taken from five different latitude bands and months, as opposed to *Toyoda et al.* [2001], which was taken from a single latitude band during a single month, the data need to be weighted appropriately in order to obtain an average of all the observations. Our weighting is by number of months and latitudes in which each set of observations was taken. Tables 2–4 also include the weighted averages of the enrichment for both model and observations.

[22] The results for the YM97 cross-sections, although following the pattern of enrichments between isotopologues

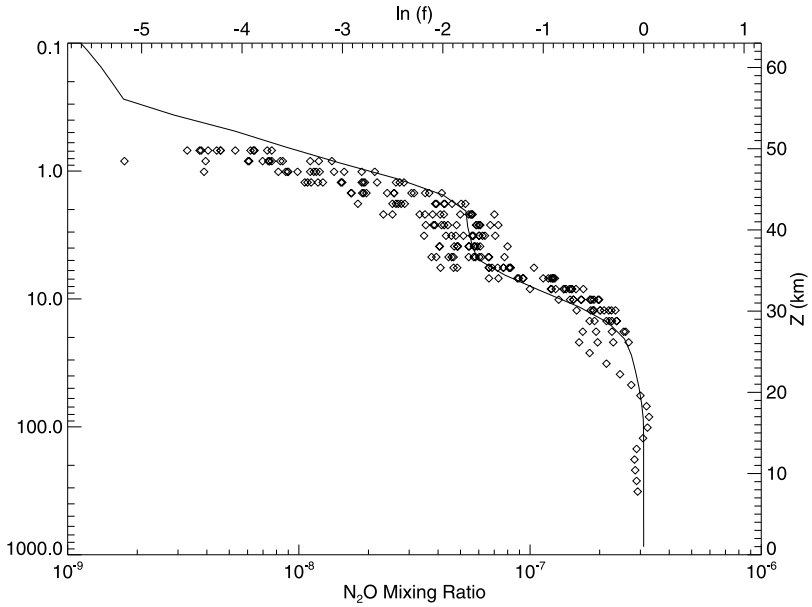

Figure 2. A comparison of observed and model concentrations of N_2O in the terrestrial atmosphere for March at 15°N. The diamonds are from the Atmospheric Trace Molecule Spectroscopy Experiment (ATMOS) campaigns. The solid line is the model concentration profile. The altitude z is defined by $z = H \ln(p_0/p)$, where H = 6.95 km, p = pressure and p_0 = 1000 mbar (see appendix A).

and isotopomers, account for less than half of the enrichment seen in observations. These results are consistent with what has been measured in laboratory studies of the isotopic fractionation of N_2O by photolysis. Cross-sections calculated by *Johnson et al.* [2001] do a better job of matching observational data, with the particular exception of (546). The (456) enrichment, while closer to observation, is still below the range of the error bars of the observations. The enrichments predicted using the cross-sections calculated by *Blake et al.* [2003] (see also Figure 1b) better match the observational data for all the isotopologues and isotopomers. However, there are major differences, namely, that *Griffith et al.*'s [2000] enrichments are all larger than the predicted values (although the error bars associated with these runs are large), while the enrichments observed using MS techniques are all smaller than the predicted values. The results of the model runs for the *Blake et al.* [2003] cross-sections agree quite well with the weighted averages of the three sets of observations.

[23] What has been observed for (447) is the excess of ^{17}O over that given by the mass dependent fractionation relation $\delta^{17}O \approx 0.515 \times \delta^{18}O$ [*Kim and Craig*, 1990; *Röckmann et al.*, 2001]. This excess has been found to be $\Delta^{17}O$ ($\delta^{17}O - 0.515 \times \delta^{18}O$) = 1.0 ± 0.2‰. For the purposes of this paper, an estimate of the observed fractionation is done using the mass-dependent fractionation relation of 0.515. In Tables 2–4, the fact that the observed fractionation of (447) is estimated is denoted by putting the values in parentheses. In the case of N_2O fractionation with $O(^1D)$ atoms, the temperature dependence of the (447) reaction is set equal to that of the (448) reaction and the logarithm of the Arrhenius A-factors for $^{14}N^{14}N^{18}O$ [see *Kaiser et al.*, 2002b, Table 2] is multiplied by the mass-dependent fractionation relation of 0.515 to determine the logarithm of the Arrhenius A-factors for $^{14}N^{14}N^{17}O$.

[24] As seen in Tables 2–4, there are discrepancies between the enrichments predicted by the model using any of the cross-section alternatives and those observed in the stratosphere. In general for the *Blake et al.* [2003] cross-sections, the enrichment predicted by the model are lower than FTS observations and higher than MS observations. However, the model matches the average of these observations. There are several possible reasons why these discrepancies are seen. First, the FTS method of retrieving the isotopic fractionation samples very long path lengths and a range of altitudes above the tangent point, and may be too sensitive to the larger signatures at higher altitudes, particularly for the optically thin isotopologue or isotopomer transitions. A second consideration is that the MS method samples more limited regions that are typically much lower in the stratosphere than the limb sounding techniques. Large sample volumes that are collected are often required, and provide another source of uncertainty that is difficult to quantify. The third possibility is that the model used has not done an adequate job of simulating the transport that influences the magnitude of the observed enrichments.

4.3. Impact of the Temperature-Dependent Cross Sections

[25] In our model the cross-sections from *Yung and Miller* [1997] and *Johnson et al.* [2001] are at room temperature. The cross-sections from *Blake et al.* [2003] are temperature-dependent. As discussed earlier, we carried out an adjustment of the cross-sections of *Blake et al.* [2003] to fit the observations of *Kaiser et al.* [2002a]. The results for enrichments computed in the model are summarized under "Modified *Blake et al.* [2003]" in Tables 2 and 4 for the upper and lower stratosphere, respectively. There is little difference between "Modified *Blake et al.* [2003]" and "*Blake et al.* [2003]" for (456). This is consistent with the good agree-

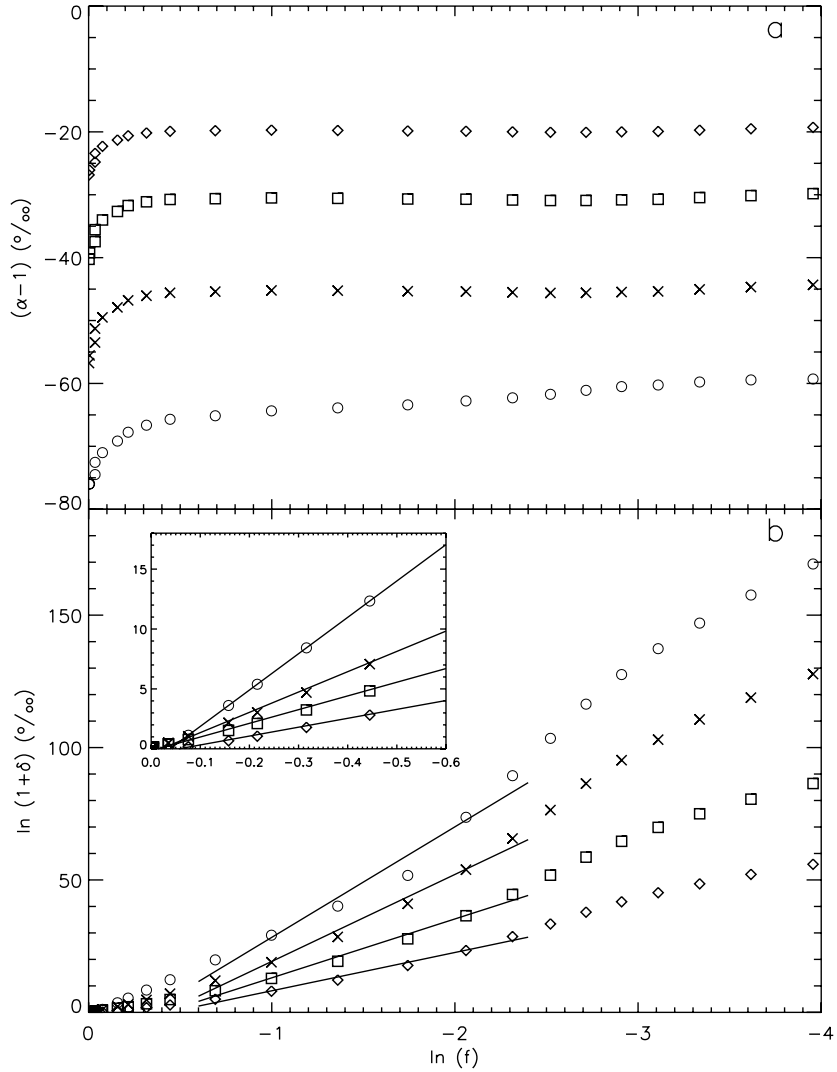

Figure 3. (a) A plot of $(\alpha_i - 1)$ versus ln f, where α_i is the ratio of the J-value for isotopologue or isotopomer i over that for (446). and f is the fraction of N_2O remaining. This plot is for May at 35°N using the theoretical cross-sections of *Blake et al.* [2003]. The symbols shown are: circles, 456; squares, 546; diamonds, 447; and crosses, 448. (b) A plot of δ versus ln f for May at 35°N using the theoretical cross-sections of *Blake et al.* [2003]. Fractionation by $O(^1D)$ is not included. The definition of δ is given in the text. The inset shows the detail of the region $0.0 > \ln F > -0.6$. The symbols shown are: circles, 456; squares, 546; diamonds, 447; and croses, 448. The slopes of solid lines are the model enrichments (ϵ). See Table 4.

ment between the model and measured temperature-dependent cross-sections. The results for (447) are also expected to be similar because there is little difference between the modified and original cross-sections. See previous section "Isotopic Fractionation of N_2O: Mechanisms and Observations." There are significant differences for the enrichment results for (546) and (448), of similar magnitude as the differences in the cross-sections. Overall, the modified *Blake et al.* [2003] cross-sections improve the agreement between the model and the MS data.

4.4. Impact of the $O(^1D)$ Channel

[26] In the 2-D model used for this paper, the contribution to fractionation by the $O(^1D)$ channel of N_2O is minimal, even in the lower stratosphere. We calculate a contribution by the $O(^1D)$ channel to the total loss rate of N_2O of around 8%, comparable to the accepted value of 10%. *Kaiser et al.* [2002b] have indicated that an important reference quantity in the lower stratosphere is the ratio $\epsilon_{456}/\epsilon_{546}$, which they designate as η. Table 5 shows a comparison of η between the three theoretical cross-sections and the average of the observations. Although η for YM97 falls within the error bars for the observations, this is only because the magnitude of the YM97 enrichment is very low compared to observations. The values of η from the theoretical cross-sections of *Johnson et al.* [2001] are much larger than observations; the greater value for η in this case is due to the very small value, compared with observations, of the enrichment for (546). The η values from the cross-sections of *Blake et al.* [2003] are larger than observations, but they fall within error bars.

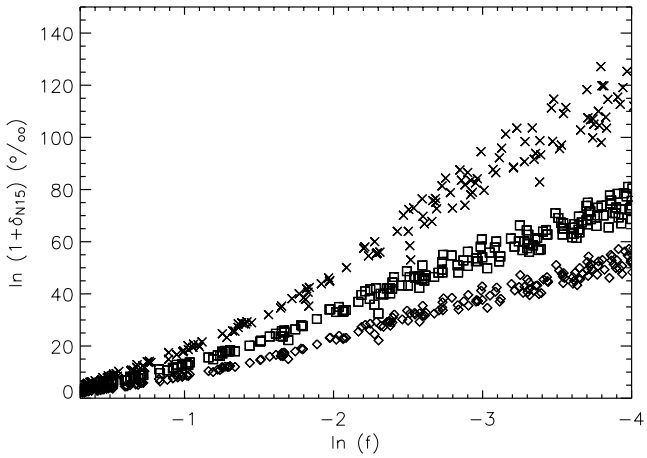

Figure 4. A plot of δ_{N15} ($\delta_{N15} = 0.5*(\delta_{456} + \delta_{546})$) versus ln *f* for months corresponding to the high latitude (65 N) observations of *Griffith et al.* [2000]. The data points correspond to the different theoretical cross-sections used in the model: diamonds, *Yung and Miller* [1997]; squares, *Johnson et al.* [2001]; crosses, *Blake et al.* [2003].

Also, the difference between runs with and without the $O(^1D)$ channel fractionation are not very great.

4.5. Chemistry Versus Transport

[27] In an effort to understand more clearly the effect of both transport and radiation on the enrichment predicted by the model, it is useful to examine these effects separately. For this purpose, the model seasonal and latitudinal variations of $(\alpha_i - 1)$ and ϵ_i are examined. The latitudinal variations of $(\alpha_i - 1)$ for (456) using the cross-sections of

Table 2. Enrichment (ε_i) for Upper Stratosphere

	YM97[a]	*Johnson et al.* [2001]	*Blake et al.* [2003]	Modified *Blake et al.* [2003]	Observations
			Midlatitude [*Griffith et al.*, 2000]		
456	−17.7 ± 0.3	−33.4 ± 0.5	−43.4 ± 1.0	−42.8 ± 1.0	−55.5 ± 9.7
546	−10.5 ± 0.2	−7.3 ± 0.1	−21.2 ± 0.5	−15.9 ± 0.4	−27.7 ± 6.7
N15	−14.1 ± 0.2	−20.3 ± 0.3	−32.3 ± 0.8	−29.3 ± 0.7	−41.3 ± 7.0
447	−7.0 ± 0.1	−13.3 ± 0.2	−13.7 ± 0.3	−13.7 ± 0.3	(−26.5 ± 4.0)
448	−13.1 ± 0.2	−25.5 ± 0.4	−31.7 ± 0.8	−26.9 ± 0.6	−51.4 ± 7.7
			High-latitude [*Griffith et al.*, 2000]		
456	−16.5 ± 0.2	−31.6 ± 0.4	−36.0 ± 0.5	−35.4 ± 0.5	−43.8 ± 3.8
546	−9.8 ± 0.1	−6.8 ± 0.1	−17.5 ± 0.2	−13.0 ± 0.2	−18.3 ± 4.0
N15	−13.2 ± 0.2	−19.2 ± 0.2	−26.8 ± 0.3	−24.2 ± 0.3	−32.7 ± 5.5
447	−6.5 ± 0.1	−12.5 ± 0.1	−11.3 ± 0.1	−11.3 ± 0.1	(−11.5 ± 2.0)
448	−12.2 ± 0.2	−24.0 ± 0.3	−26.2 ± 0.3	−22.2 ± 0.3	−22.3 ± 3.9
			Röckmann et al. [2001]		
456	−17.8 ± 0.2	−32.3 ± 0.3	−47.2 ± 0.5	−47.1 ± 0.5	−32.3 ± 1.2
546	−10.5 ± 0.1	−7.2 ± 0.1	−23.1 ± 0.3	−17.6 ± 0.2	−16.0 ± 0.6
N15	−14.1 ± 0.1	−19.8 ± 0.2	−35.2 ± 0.4	−32.3 ± 0.4	−24.3 ± 0.7
447	−6.9 ± 0.1	−12.8 ± 0.1	−14.8 ± 0.2	−14.9 ± 0.2	(−10.9 ± 0.3)
448	−13.1 ± 0.1	−24.9 ± 0.2	−34.9 ± 0.4	−29.4 ± 0.3	−21.0 ± 0.6
			Toyoda et al. [2001]		
456	−21.2 ± 0.2	−38.0 ± 0.3	−55.0 ± 0.7	−54.8 ± 0.7	−40.9 ± 1.3
546	−12.5 ± 0.1	−8.5 ± 0.1	−26.9 ± 0.3	−20.5 ± 0.3	−15.5 ± 0.4
N15	−16.8 ± 0.1	−23.3 ± 0.2	−40.9 ± 0.5	−37.6 ± 0.5	−28.6 ± 0.6
447	−8.2 ± 0.1	−15.2 ± 0.1	−17.2 ± 0.2	−17.2 ± 0.2	(−12.7 ± 0.3)
448	−15.6 ± 0.1	−29.5 ± 0.2	−40.6 ± 0.5	−34.1 ± 0.4	−24.6 ± 0.6
			Weighted Average		
456	−17.6 ± 0.2	−32.7 ± 0.4	−43.5 ± 0.6	−43.1 ± 0.6	−40.7 ± 3.5
546	−10.4 ± 0.2	−7.2 ± 0.1	−21.2 ± 0.3	−16.0 ± 0.2	−18.7 ± 2.7
N15	−14.0 ± 0.2	−20.0 ± 0.2	−32.4 ± 0.4	−29.5 ± 0.4	−30.3 ± 3.3
447	−6.9 ± 0.1	−13.0 ± 0.1	−13.7 ± 0.2	−13.7 ± 0.2	(−13.8 ± 1.7)
448	−13.0 ± 0.2	−25.1 ± 0.3	−31.9 ± 0.4	−27.0 ± 0.4	−26.8 ± 2.9

[a]YM97, *Yung and Miller* [1997]; N15 = $(\delta_{456} + \delta_{546})/2$.

Table 3. Enrichment (ε_i) for Lower Stratosphere–Fractionation by $O(^1D)$ Not Included in Model

	YM97[a]	*Johnson et al.* [2001]	*Blake et al.* [2003]	Observations
		Rahn and Wahlen [1997]		
N15	−7.6 ± 0.1	−11.7 ± 0.1	−16.5 ± 0.1	−14.5
447	−3.6 ± 0.1	−7.4 ± 0.1	−6.8 ± 0.1	(−6.6)
448	−6.7 ± 0.1	−14.2 ± 0.1	−15.8 ± 0.1	−12.9
		Röckmann et al. [2001]		
456	−9.6 ± 0.1	−19.6 ± 0.2	−23.4 ± 0.2	−20.9 ± 1.5
546	−5.4 ± 0.1	−3.8 ± 0.1	−11.0 ± 0.1	−12.7 ± 2.4
N15	−7.5 ± 0.1	−11.7 ± 0.1	−17.2 ± 0.2	−16.8 ± 1.6
447	−3.5 ± 0.1	−7.4 ± 0.1	−7.1 ± 0.1	(−7.1 ± 1.0)
448	−6.7 ± 0.1	−14.1 ± 0.1	−16.4 ± 0.2	−13.8 ± 2.0
		Toyoda et al. [2001]		
456	−9.0 ± 0.1	−18.3 ± 0.2	−21.8 ± 0.2	−22.9 ± 1.2
546	−5.1 ± 0.1	−3.6 ± 0.1	−10.2 ± 0.1	−8.8 ± 1.4
N15	−7.0 ± 0.1	−11.0 ± 0.1	−16.0 ± 0.2	−15.9 ± 1.1
447	−3.3 ± 0.1	−7.0 ± 0.1	−6.6 ± 0.1	(−5.9 ± 0.9)
448	−6.3 ± 0.1	−13.2 ± 0.1	−15.2 ± 0.1	−11.5 ± 1.8
		Weighted Average		
456	−9.5 ± 0.1	−19.4 ± 0.2	−23.1 ± 0.2	−21.2 ± 1.5
546	−5.4 ± 0.1	−3.8 ± 0.1	−10.9 ± 0.1	−12.0 ± 2.2
N15	−7.5 ± 0.1	−11.6 ± 0.1	−16.8 ± 0.2	−15.4 ± 1.5
447	−3.5 ± 0.1	−7.4 ± 0.1	−6.9 ± 0.1	(−6.8 ± 1.0)
448	−6.7 ± 0.1	−14.1 ± 0.1	−16.0 ± 0.2	−13.2 ± 2.0

[a]YM97, *Yung and Miller* [1997]; N15 = $(\delta_{456} + \delta_{546})/2$.

Table 4. Enrichment (ε_i) for Lower Stratosphere–Fractionation by $O(^1D)$ Included

	YM97[a]	*Johnson et al.* [2001]	*Blake et al.* [2003]	Modified *Blake et al.* [2003]	Observations
			Rahn and Wahlen, [1997]		
N15	−7.8 ± 0.1	−12.0 ± 0.1	−16.7 ± 0.1	−14.9 ± 0.1	−14.5
447	−3.9 ± 0.1	−7.8 ± 0.1	−7.1 ± 0.1	−7.1 ± 0.1	(−6.6)
448	−7.3 ± 0.1	−14.8 ± 0.1	−16.2 ± 0.1	−13.8 ± 0.1	−12.9
			Röckmann et al. [2001]		
456	−9.7 ± 0.1	−19.7 ± 0.2	−23.5 ± 0.2	−22.8 ± 0.2	−20.9 ± 1.5
546	−5.9 ± 0.1	−4.2 ± 0.1	−11.4 ± 0.1	−8.3 ± 0.1	−12.7 ± 2.4
N15	−7.8 ± 0.1	−12.0 ± 0.1	−17.5 ± 0.2	−15.6 ± 0.2	−16.8 ± 1.6
447	−3.9 ± 0.1	−7.8 ± 0.1	−7.4 ± 0.1	−7.4 ± 0.1	(−7.1 ± 1.0)
448	−7.3 ± 0.1	−14.8 ± 0.1	−16.9 ± 0.2	−14.4 ± 0.1	−13.8 ± 2.0
			Toyoda et al. [2001]		
456	−9.1 ± 0.1	−18.4 ± 0.2	−21.9 ± 0.2	−21.2 ± 0.2	−22.9 ± 1.2
546	−5.5 ± 0.1	−4.0 ± 0.1	−10.6 ± 0.1	−7.7 ± 0.1	−8.8 ± 1.4
N15	−7.3 ± 0.1	−11.2 ± 0.1	−16.2 ± 0.2	−14.5 ± 0.1	−15.9 ± 1.1
447	−3.6 ± 0.1	−7.3 ± 0.1	−6.9 ± 0.1	−6.9 ± 0.1	(−5.9 ± 0.9)
448	−6.8 ± 0.1	−13.9 ± 0.1	−15.8 ± 0.1	−13.4 ± 0.1	−11.5 ± 1.8
			Weighted Average		
456	−9.6 ± 0.1	−19.5 ± 0.2	−23.2 ± 0.2	−22.5 ± 0.2	−21.2 ± 1.9
546	−5.8 ± 0.1	−4.2 ± 0.1	−11.3 ± 0.1	−8.2 ± 0.1	−12.0 ± 1.8
N15	−7.8 ± 0.1	−11.9 ± 0.1	−17.1 ± 0.2	−15.2 ± 0.2	−15.4 ± 1.9
447	−3.9 ± 0.1	−7.8 ± 0.1	−7.2 ± 0.1	−7.2 ± 0.1	(−6.8 ± 1.3)
448	−7.3 ± 0.1	−14.7 ± 0.1	−16.5 ± 0.2	−14.1 ± 0.1	−13.2 ± 2.0

[a]YM97, *Yung and Miller* [1997]; N15 = $(\delta_{456} + \delta_{546})/2$. Our model also matches observations made by *Yoshida and Toyoda* [2000] (derived by *McLinden et al.* [2003]) for the month of September at 40 N in the lower stratosphere. Model ϵ for (456), (546), (448) are −24.0, −11.7, and −17.4; observational ϵ are −24.5, −13.9, and −17.0.

Table 5. η-Factors for Lower Stratosphere

	YM97	*Johnson et al.* [2001]	*Blake et al.* [2003]	Observations (Weighted Average)
η[incl. $O(^1D)$ channel]	1.65 ± 0.12	4.64 ± 0.28	2.05 ± 0.08	1.77 ± 0.30
η[w/out $O(^1D)$ channel]	1.76 ± 0.05	5.10 ± 0.17	2.12 ± 0.08	1.77 ± 0.30

Blake et al. [2003] are shown in Figure 5. The variations for the other isotopologues or isotopomers are similar to (456) except for their magnitude. The quantity $(\alpha_i - 1)$ becomes ill-defined in the polar region during local winter (July in the South, January in the North) due to the vanishing solar flux. For the purposes of this figure, all $J_i < 10^{-10}$ s^{-1} are ignored. There is little variation between 50°S and 50°N regardless of the season. This is to be expected because there is little variation in the spectral distribution of the solar flux in this zonal region and between seasons. One aspect of $(\alpha_i - 1)$ that needs further explanation is its marked increase in the region near the poles. This increase can be explained if the wavelength dependence of the solar fluxes between the tropics and the high latitudes is examined. There is more solar flux at wavelengths less than 200 nm in the tropics than in the high latitudes. The reason for this change in flux is the greater attenuation by O_2 at higher latitudes. For wavelengths greater than 200 nm, the difference in solar flux between the tropics and the high latitudes is not as great. In the shorter wavelength region, however, the fractionation constants are very low compared to longer wavelengths, and thus the rate of fractionation by photolysis will be greater near the poles than at the tropics.

[28] Although the results obtained in this work are based on a 2-D model, we can nevertheless gain some insight into the effect of transport on ϵ_i by considering an analytic 1-D model with transported parameterized by eddy diffusion [*Kaye*, 1987; *Rahn et al.*, 1998]. See appendix B for details. The relation between α_i, and ϵ_i in this simple model is given by

$$\varepsilon_i = (\alpha_i - 1)E \tag{9}$$

$$E = \frac{1}{2}\left(1 + \sqrt{\frac{r}{1+r}}\right) \tag{10}$$

where $r = \tau_{chem}/4\tau_{trans}$ with τ_{chem} = chemical lifetime = $1/J$ and τ_{trans} = transport time. The transport time in the 1-D model is parameterized by H^2/K_1 where H is the scale height and K_1 is the eddy diffusion coefficient in the stratosphere. Note that K_1 must not be confused with the K_{zz} in equation (7). K_1 is much larger than K_{zz} because it includes, at least approximately, all transport processes by advection and diffusion. The estimates in appendix B suggest r = 0.38 and E = 0.76. The 1-D model also yields a simple relation between ε_i and $\delta\tau_i$, the difference in the mean lifetime between the isotopologue or isotopomer (i) and the most abundant isotopologue $\delta\tau_i = -\varepsilon_i$. These relations will be useful for interpreting the results from the 2-D model.

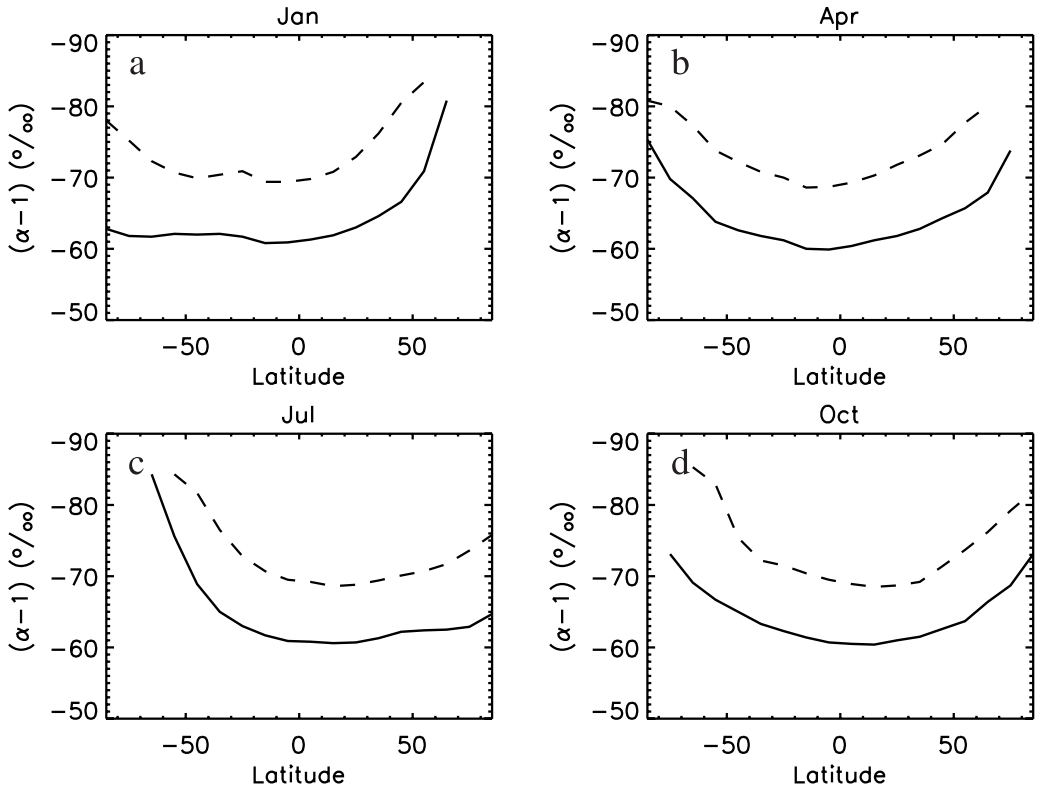

Figure 5. A plot of model-determined $(\alpha_{456} - 1)$ as a function of latitude for four months: (a) January, (b) April, (c) July, and (d) October. The dashed lines are for the lower stratosphere $(0.0 < \ln f < -0.6)$. The solid lines placed are for the upper stratosphere $(-0.6 < \ln f < -4.0)$.

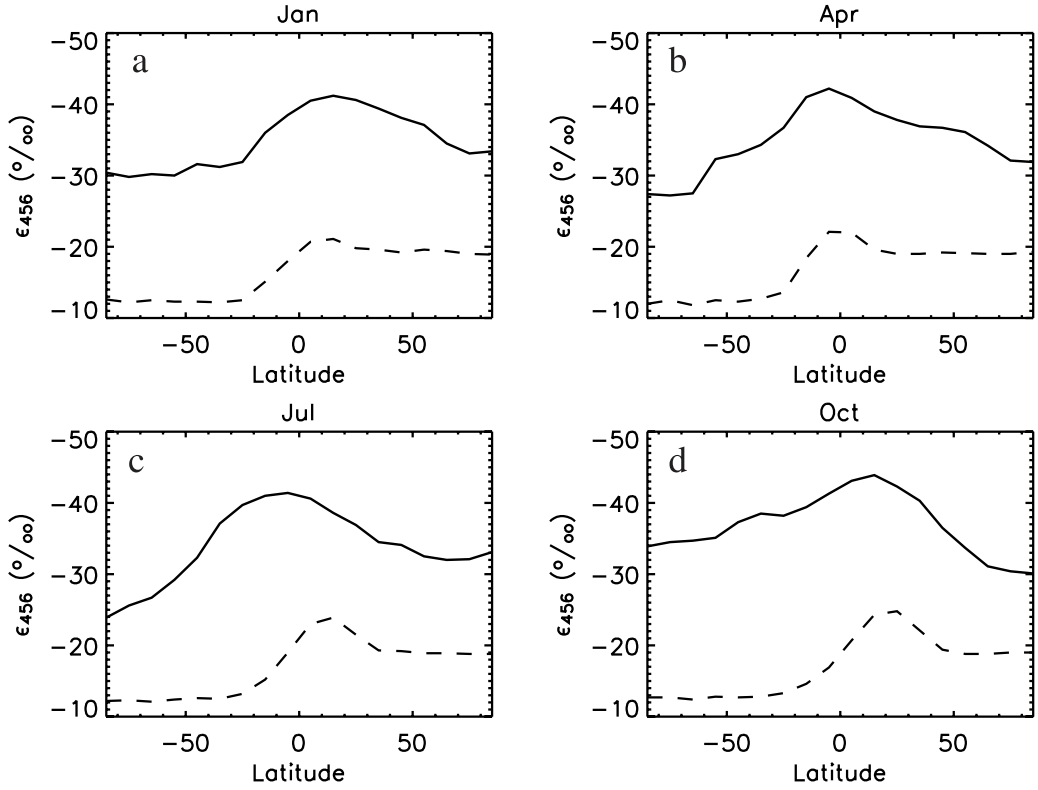

Figure 6. A plot of model-determined enrichments (ϵ_{456}) as a function of latitude for four months: (a) January, (b) April, (c) July, and (d) October. The dashed lines are for the lower stratosphere ($0.0 < \ln f < -0.6$). The solid lines are for the upper stratosphere ($-0.6 < \ln f < -4.0$).

[29] The model results for ϵ_{456} are presented in Figure 6. There are striking latitudinal and seasonal variations, which can be attributed to transport. These enrichments were computed using the cross-sections of *Blake et al.* [2003]. The variations in ϵ_i for the other isotopologues and isotopomers are also similar to those of ϵ_{456} except for their magnitudes. There is a large increase in ϵ_i in the tropics. This increase in ϵ_i reflects upwelling in the tropics. As demonstrated with our 1-D diffusion model, an increase in vertical transport results in an increase in isotopic enrichment. The width of the upwelling region also varies seasonally; it is narrowest in April and widest in October.

4.6. N_2O Production by Nonstandard Chemistry

[30] *Zipf and Prasad* [1998] presented evidence for a nonstandard source of N_2O in the atmosphere via excited state chemistry. The reactions leading to the production of N_2O can be schematically summarized by

$$O + O_2 + N_2 \rightarrow O_2 + N_2O \qquad (11)$$

The quantum yield of (11) may be written as $Q = Q_{ZP} \times \beta$, where Q_{ZP} was estimated using laboratory experiments and $\beta < 1$ is a further reduction factor introduced by us. A quantitative assessment of the impact of this hypothetical source of N_2O was carried out with $\beta = 0.03$. See appendix C for details. The new source amounts to 1.53 Tg N yr^{-1} and increases the mixing of N_2O through out the atmosphere by about 10%. However, the new source also increases δ_{448} by more than 10‰ in the troposphere as well as the stratosphere! This is clearly a violation of the present observations because this implies a large unknown biological source of very small δ_{448}. The source from nonstandard chemistry must be much smaller than that computed in our model.

4.7. Implications for the Biosphere

[31] The total loss rates for the major isotopologue of N_2O (molecules $cm^{-3}s^{-1}$) as a function of altitude and latitude for the four seasons are shown in Figure 7. The bulk of N_2O destruction occurs in the mid stratosphere, and the maximum destruction rate follows the sun. The total atmosphere-integrated mass is 1489 Tg N. The annually averaged integrated loss rate is 9.2828×10^{27} molecules s^{-1}, or 13.6 Tg N yr^{-1}. The mean lifetime for N_2O is 109 yrs. These values are close to those in the literature [see, e.g., *Houghton et al.*, 2001]. The annually averaged integrated loss rates for isotopologues (456), (546), (447) and (448) are 3.3735×10^{25}, 3.4063×10^{25}, 3.4442×10^{24} and 1.8744×10^{25}, molecules s^{-1}, respectively. On a per molecule basis, the rates of destruction of the minor isotopologues are somewhat less than that for the major isotopologue. From the above we derive the relative rates for (446), (456), (546), (447) and (448), to be 1, 0.9843, 0.9942, 0.9949, and 0.9900, respectively. Thus the destruction of N_2O in the atmosphere results in the isotopic fractionation of the minor isotopologues (456), (546), (447) and (448) by 19.4, 9.5, 5.5 and 12.0‰, respectively. If we do not distinguish between (456) and (546), we obtain 14.5‰ as the mean isotopic fractionation for the two isotopomers.

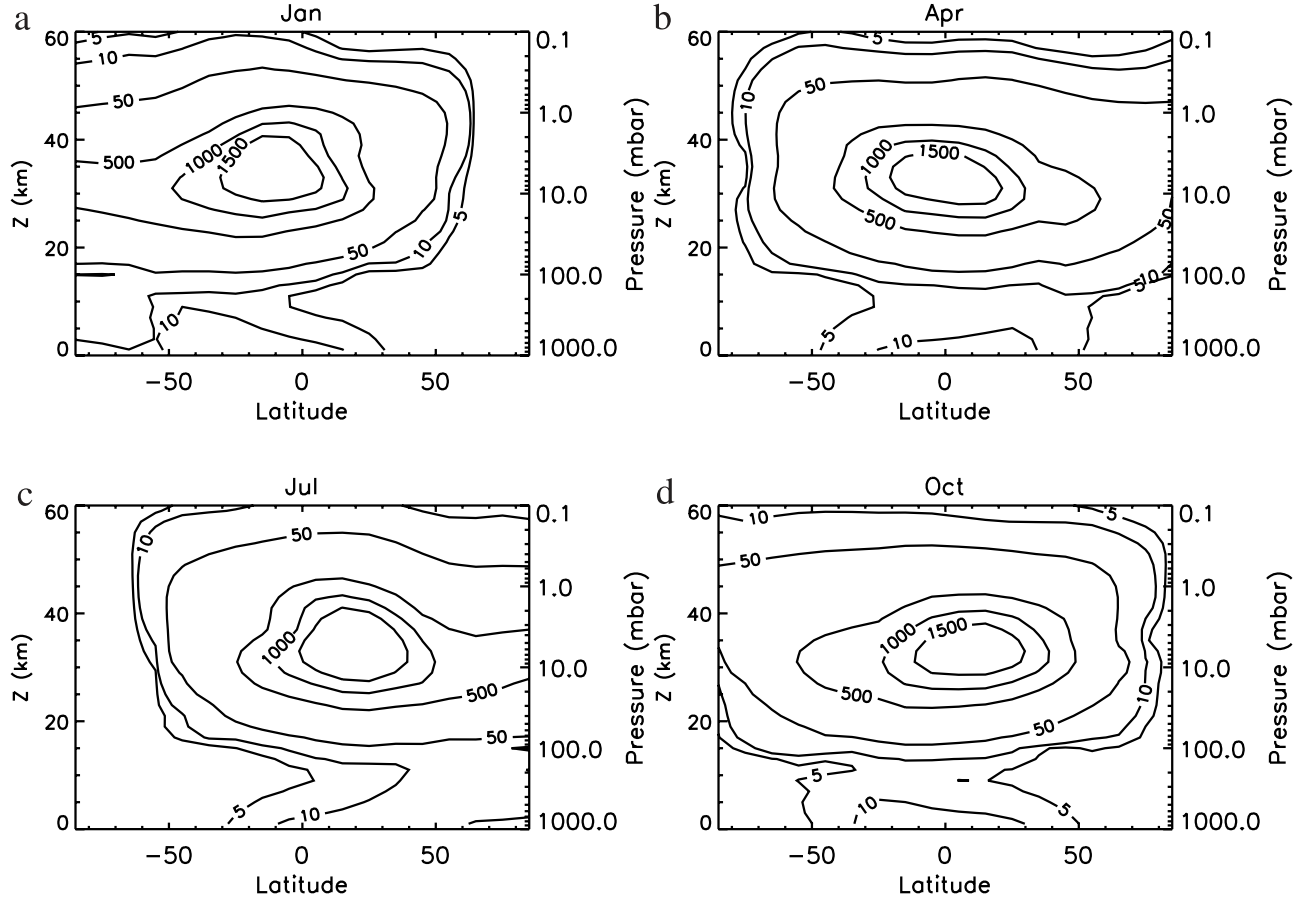

Figure 7. The total N_2O loss rate as a function of altitude and latitude, (a) January, (b) April, (c) July, and (d) October. The units are in molecules cm^{-3} s^{-1}.

[32] The enrichment values for whole atmosphere obtained above will be compared with previous results reported by *Morgan et al.* [2002] and *Yung* [2002]. *Yung* [2002] is the first to publish these quantitative results using the cross-sections of *Blake et al.* [2003] and an earlier version of the Caltech/JPL 2-D model. The results are summarized in Table 6. *McLinden et al.* [2003] obtained similar results using the cross-sections of *Yung and Miller* [1997] with scaling and *Johnson et al.* [2001] in a 3-D model. A detailed examination of Table 6 shows that the results in their second model (after adjustment for (546)) and *Yung* [2002] are within 1.1‰ for all isotopologues and isotopomers. This is a remarkable coincidence in view of the acknowledged numerical problems of the 3-D model in question (see appendix A) and the fact that we are comparing 2-D and 3-D models with very different physics. It is very important that the results of *McLinden et al.* [2003] be reproduced with an isentropic model with proven numerical stability and validated age of air. The new results in this paper are summarized in Table 6. The main difference between these and those of *Yung* [2002] is that the present model used the NCEP-derived circulation, whereas *Yung* [2002] used an older UARS-derived circulation. The two new results reflect the impact of the temperature dependent cross-sections measured by *Kaiser et al.* [2002a]. It remains a challenge for the 3-D model to reproduce these results.

[33] The implications of these calculations for biospheric sources of N_2O are discussed below. From the extensive measurements available for $\delta^{18}O$ and $\delta^{15}N$, mean tropospheric fractionation values of 20.7 and 7.0‰, respectively, are found (KC93). Therefore to balance the budgets for the isotopic composition of N_2O, the $\delta^{18}O$ and $\delta^{15}N$ for the integrated sources must be 6.3 and −7.9‰, respectively. There are fewer tropospheric measurements that distinguish between the (456) and (546) isotopomers. *Yoshida and Toyoda* [2000] reported a large site preference for the center ^{15}N, $\delta_{456} - \delta_{546} = 18.7 \pm 2.2$‰. Since atmospheric chemistry can account for only 19.4–9.5 = 9.9‰, the mean source of N_2O must have $\delta_{456} - \delta_{546} = 18.7 - 9.9 \pm 2.2 = 8.8 \pm 2.2$‰. From the preceding discussion of $\delta^{15}N$, we have $\delta_{456} + \delta_{546} = -14.5$‰. Solving these two equations, we obtain $\delta_{456} = -2.9 \pm 1.1$‰ and $\delta_{546} = -11.7 \pm 1.1$‰. This provides a quantitative evaluation of the isotopic composition of the integrated sources of N_2O. Further measurements, especially for the (447) isotopologue and

Table 6. Enrichment (ε_i) for Whole Atmosphere

Isotopologue/ Isotopomer	*Yung* [2002]	*McLinden et al.* [2003]	*McLinden et al.* [2003]	*Blake et al.* [2003]	Modified *Blake et al.* [2003]
456	−20.0	−14.2	−19.1	−20.0	−19.4
546	−9.7	−8.2	−4.0 (−10.9)	−11.6	−9.5
447	−6.3	−5.4	−7.3	−5.5	−5.5
448	−14.4	−10.0	−13.9	−13.8	−12.0

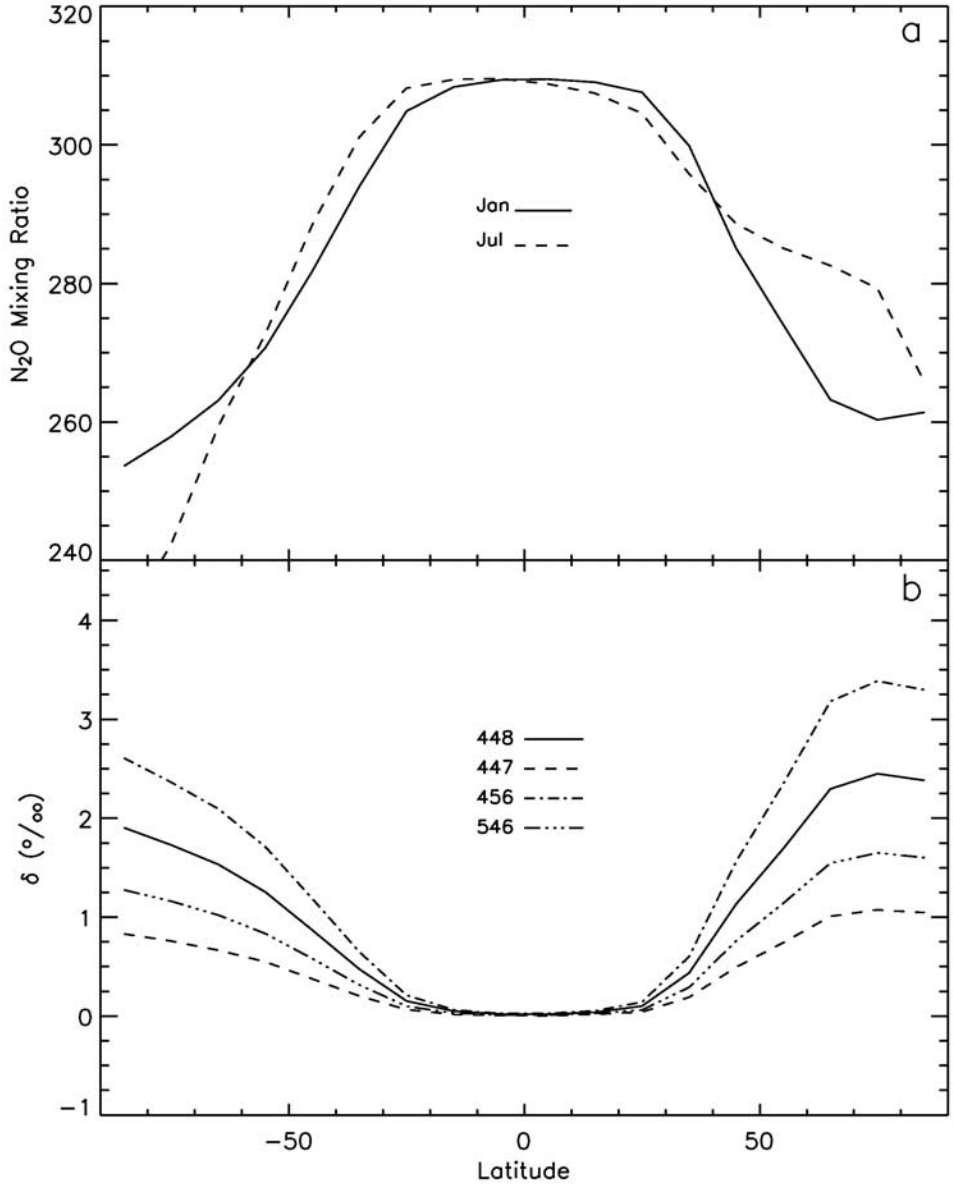

Figure 8. (a) Mixing ratio of N_2O at 100 mbar as a function of latitude for January and July. (b) Isotopic fractionation for N_2O isotopologues and isotopomers at 100 mbar as a function of latitude in January.

the isotopic signature of biological sources, are needed to verify and refine these results.

4.8. Implications for Atmospheric Measurements

[34] Some critical aspects of the model results can be tested by atmospheric measurements. The model has two independent components, chemistry and transport. Since the chemistry is the same for all five isotopologues and isotopomers of N_2O, it is easier to get the correct chemistry relative to each other. As the chemical network becomes more precise, the measurements will be useful for refining our understanding of the transport processes, especially on seasonal and interannual timesales.

[35] Figure 8a presents the latitudinal distributions of the mixing ratio of N_2O at 100 mbar, which is close to the pressure of the tropopause in the tropics. As discussed earlier, the air in the tropics ascends from the troposphere to the stratosphere. The tropical mixing ratio of N_2O is close to the surface value of 310 ppbv. At higher latitudes, the mixing ratio of N_2O is 20–40 ppbv less than those in the tropics because the air is returning from high altitudes where destruction of N_2O by photolysis has occurred. These results are consistent with KC93's estimate of ~15 ppbv N_2O mixing ratio difference between the upwelling and downwelling regions at 100 mbar. The main differences between the winter and summer months in their respective hemispheres are photolysis (stronger in summer) and transport (stronger in winter). The effect of transport clearly overwhelms that of chemistry. To our knowledge, there has not been a systematic mapping of the latitudinal distribution of N_2O near the tropopause region for different seasons. Such measurements will provide further quantitative testing of the model.

[36] Figure 8b presents the latitudinal distributions of the isotopic fractionations of N_2O isotopologues and

isotopomers at 100 mbar in January. Relative to the air that enters the stratosphere, the air that returns from the stratosphere is enriched in the minor isotopologues and isotopomers, as first pointed out by KC93 and discussed in the Introduction. A systematic mapping of the latitudinal and seasonal pattern of the δ values near the tropopause will provide further confirmation of the model predictions.

[37] In the middle and upper stratosphere the transport is uncertain for both 2-D and 3-D models. See appendix A for details. It is important to obtain simultaneous measurements of N_2O isotopologues and isotopomers and the age of air to constrain the models.

4.9. Comparison With KC93

[38] KC93 provide the first simple and elegant analysis of the budget of N_2O isotopologues in terms of exchange between the troposphere and the stratosphere. While our 2-D model computes all physical and chemical processes with detailed spatial and temporal resolution, it is nevertheless useful to visualize the overall results by taking annual averages and averages over the troposphere and the stratosphere. For this simple box model analysis, we assume that the troposphere (stratosphere) is the region below (above) 100 mbar.

[39] Adopting the concepts and methodology of KC93, the steady state tropospheric isotopic flux balance is

$$S_i\Delta_i + F^u\delta_t - F^d\delta_{st} = 0 \qquad (12)$$

where S_i and δ_i are the source flux and isotopic fractionation of the surface source, $\Delta_i = \delta_i - \delta_t$ = difference between the source and the tropospheric isotopic fractionation, F^u, F^d = flux of N_2O to and from the stratosphere, δ_{st} = isotopic fractionation in the stratosphere. We will give an illustration of the balance implied by equation (12) for the (448) isotopologue. The values for the annually averaged F^u and F^d are 71 and 59 Tg N yr^{-1}, respectively. Note that most of the N_2O that gets transported into the stratosphere returns to the troposphere. Only about 17% is destroyed. To compare with Equation (1) in KC93, we have to make the approximation that $F^u \approx F^d = F_{st}$. In this case (12) becomes

$$S_i\Delta_i + F_{st}\Delta_{st} = 0 \qquad (13)$$

where $\Delta_{st} = \delta_{st} - \delta_t$. Equation (13) is identical to equation (1) in KC93, except that we denote the source flux by S_i instead of J_i, and that we drop the summation symbol for simplicity. Equation (12) is rigorously correct, while equation (13) is approximate. From our model, we have $F_{st} \approx 64$ Tg N yr^{-1}, $\Delta_{st} \approx 2.9$‰. Therefore we have $F_{st}\,\Delta_{st} \approx 190$ Tg N yr^{-1}‰. KC93 obtained 500 Tg N yr^{-1}‰. The reason for the discrepancy is not hard to find. KC93 assumed $F_{st} \approx 60.5$ Tg N yr^{-1}, which is very close to our value. However, they assumed $\Delta_{st} \approx 8$‰, based on their single measurement at 68°N. This value is not representative of the isotopic fractionations for (448) shown in Figure 8b. Since there is no known source that can account for 500 Tg N yr^{-1}‰, KC93 speculated that there might be large oceanic fluxes. The smaller fluxes obtained by our model make such speculation unnecessary. Further measurements in the down-welling regions are needed to resolve this discrepancy between KC93 and our model.

4.10. Causes for the Increase of Atmospheric N_2O

[40] As pointed out in the Introduction, the outstanding problem in N_2O is to find the causes for the increase of atmospheric N_2O by 11% since the Pre-Industrial Revolution (PIR) and by 44% from the Last Glacial Maximum (LGM) to PIR. Recently, *Röckmann et al.* [2003] determined the isotopic fractionation in N_2O in Antarctic firn samples. The decrease from PIR to the present are $\delta_{456} = -2.2$‰, $\delta_{546} = -1.8$‰, and $\delta_{448} = -1.2$‰. This pattern of change suggests that enhanced biological emission associated with agriculture is a likely explanation [*Rahn and Wahlen*, 2000]. Additionally, there has not been a drastic climate change in the last few centuries. The causes for the low concentrations of N_2O during LGM may be more complex. *Yung et al.* [1996] argued that there was a major climate regime change. An enhanced Brewer-Dobson circulation could result in a faster transport of N_2O to the stratosphere and this implies a greater sink for N_2O. What would be the isotopic signature? As a concrete example, let us speculate that half of the 44% increase from LGM to PIR is due to a slowing down of the Brewer-Dobson circulation. Using the ideas outlined in this work, we estimate the following increase from LGM to PIR, $\delta_{456} = 1$‰, $\delta_{546} = 0.5$‰, $\delta_{447} = 0.3$‰ and $\delta_{448} = 0.7$‰. Note that δ_{456} and δ_{456} are different, because they bear the signature of the stratosphere. However, the numbers are smaller than those from the biological sources and are of the opposite sign. It remains a challenge to the experimentalists to extract this interesting information on longer timescales [*Röckmann et al.*, 2003].

5. Conclusions

[41] A 2-D chemical tracer model simulation of N_2O isotope fractionation in the stratosphere using three sets of theoretical cross-sections for N_2O photolysis, shows that the semi-empirical approach of *Blake et al.* [2003] most closely matches all available observations. The *ab initio* approach of *Johnson et al.* [2001] does an excellent job of matching observations for $^{14}N^{14}N^{18}O$, but it has more difficulty with the ^{15}N-substituted isotopologues and isotopomers. The inclusion of isotope fractionation of N_2O through its reaction with $O(^1D)$ does not make a significant contribution to overall fractionation in the stratosphere, but the use of the correct temperature dependence for the cross-sections [*Kaiser et al.*, 2002a] is shown to be important. A study of the seasonal and latitudinal variation in the enrichments, i.e., the rates of fractionation, shows variations in the tropics and midlatitudes that can be attributed to transport phenomena, while variations in the polar regions can be attributed to changes in radiation.

[42] This work essentially completes the program for the atmospheric study of isotopic fractionation of N_2O envisioned by KC93. The destruction of N_2O in the stratosphere results in the enrichment of its heavier isotopologues and isotopomers. The 2-D model can quantitatively account for the observed enrichments based on the best photochemical and kinetics data. The 2-D and 3-D [*McLinden et al.*, 2003] results generally agree. There remain major uncertainties in

the transport in the upper stratosphere. New simultaneous measurements of the isotopologues and isotopomers of N_2O and the age of air are needed to constrain the models. The back flux of N_2O from the stratosphere to the troposphere, occurring primarily at high latitudes, is a source of heavy N_2O to the troposphere. There appears to be some discrepancy in the magnitude of the isotopic source strengths, as defined by Equation (13). KC93 reported a value of 500 Tg N yr^{-1}‰, which is much larger than the model prediction of 190 Tg N yr^{-1}‰. Additional measurements in the lower stratosphere are needed to improve our understanding.

[43] It is shown that nonstandard sources of N_2O are unlikely to exceed about 10% of the currently known sources. The cause for the increase of N_2O in the atmosphere since the ice age is most likely biological emission. However, we speculate that there might be a contribution from a change in the stratospheric sink as a result of an atmospheric circulation regime shift. These two causes have distinctive isotopic signatures, especially in (456) and (546).

Appendix A: The Caltech/JPL 2-D Model

[44] The Caltech/JPL 2-D Model is a zonally averaged two-dimensional (2-D) model for trace species in the terrestrial troposphere and middle atmosphere [*Shia et al.*, 1989]. It is derived from the Caltech/JPL 1-D Model [*Allen et al.*, 1981]. The focus of our modeling effort is the simulation of the spatial distribution and temporal variation of chemical species in the atmosphere. Our model aims at integrating the information obtained by laboratory studies and atmospheric observations to achieve a quantitative understanding of the chemical, radiative and dynamical processes that are relevant to a realistic evaluation of human impact on the global environment. In the current operating mode it is a time dependent model of the global atmosphere in latitude and pressure, composed of four modules: the chemical module, the solar radiative module, the infrared radiative module, and the transport module.

[45] The dimensions in the model are arbitrary. The horizontal coordinate in the model is $y = a\theta$, where a = planetary radius and θ = latitude. In this study, there are 18 latitude boxes, equally spaced from pole to pole. The vertical coordinate is log pressure, given by $z = H \ln(p_0/p)$, where $H = 16 \times \ln(10) = 6.949$ km, p = pressure and p_0 = surface pressure = 1000 mbar. The value for H is approximately the mean scale height of the atmosphere and yields z = 80 km for p = 0.01 mbar. For the present computations, the model has 40 layers, equally spaced from the surface to the upper boundary at 0.01 mbar. The tropopause (independent of season) is approximated by p = 100 mbar between 30°S and 30°N, p = 300 mbar poleward of 60°, and p = 200 mbar between 30° and 60°.

[46] The continuity equation

$$\frac{\partial \chi}{\partial t} + v\frac{\partial \chi}{\partial y} + w\frac{\partial \chi}{\partial z} - \frac{1}{\cos\theta}\frac{\partial}{\partial y}\left\{\cos\theta K_{yy}\frac{\partial \chi}{\partial y}\right\} - e^{\xi}\frac{\partial}{\partial z}\left\{e^{-\xi}K_{zz}\frac{\partial \chi}{\partial z}\right\} = \frac{Q}{M} \quad \text{(A1)}$$

is solved for all long-lived species, where χ is the mixing ratio for the species; $\xi = z/H$, and *5*, *w*, K_{yy} and K_{zz} denote the horizontal velocity, vertical velocity, horizontal eddy diffusivity, and vertical eddy diffusivity, respectively. Q is the net chemical production rate and M is the number density of the ambient atmosphere. Until recently, the advection used in the model is the "residual mean circulation" derived from diabatic heating [*Garcia and Solomon*, 1983; *Ko et al.*, 1985]. The horizontal eddy diffusivity, K_{yy}, is self-consistently computed from the momentum equation [*Tung*, 1982]. K_{zz} is an adjustable parameter in the model, but is set to a small value so that it does not play a crucial role in the transport of species in the troposphere and stratosphere. The input data used for the computation of the transport fields (5, w, K_{yy}) are taken from UARS observations for 1992 [*Eluszkiewicz et al.*, 1996] above 250 mbar. Below 250 mbar we adopt transport fields that have been tested using tracers in the troposphere [*Brown*, 1993]. The values for K_{zz} are taken from *Summers et al.* [1997]. They are not important except in the mesosphere. Recently, we added a new option to derive the 2-D advection from the National Center for Climate Prediction (NCEP) 3-D winds [*Jiang et al.*, 2003, manuscript in preparation, 2003]. The advantages of the NCEP-derived advection are twofold. First, it unifies the troposphere transport (the Hadley circulation) and the stratospheric transport (Brewer-Dobson circulation). Second, it has the realism of assimilated data. However, the NCEP data are not accurate above 40 km, where we adopt the climatologically averaged circulation derived by *Fleming et al.* [2002] for the Goddard Space Flight Center (GSFC) 2-D model. There is a gradual merging of the two between 30 and 40 km.

[47] The model includes all the gas phase chemistry in the NASA recommendations for stratospheric modeling [*DeMore et al.*, 1997]. Long-lived species are fixed at the ground at concentrations given by observations in 1986, as summarized in Table A1. The surface concentrations of species that have strong latitudinal gradients are presented in Table A2. The choice of 1986 as the "standard atmosphere" is motivated by the fact that it is often the starting point for decadal time dependent perturbation studies of the atmosphere. The model posits 2.65 ppbv of chlorine, 0.93 ppbv of fluorine and 15 pptv of bromine. All the important species in the major families are calculated individually without further approximation. These include the oxygen group (O, $O(^1D)$ and O_3), the hydrogen group (H, OH, HO_2, H_2O_2, H_2), the methane group (CH_3, CH_3O, CH_3O_2, CH_3OOH, HCO, H_2CO, CO and CH_4), the nitrogen group (N, NO, NO_2, NO_3, N_2O_5, HNO_3, HO_2NO_2 and N_2O), the chlorine group (Cl, ClO, HOCl, $ClONO_2$, HCl, OClO and CFCs), the bromine group (Br, Br_2, BrO,

Table A1. Mixing Ratios of Long-Lived Species at the Surface

Species	Mixing ratio	Species	Mixing Ratio
O_3	3.0×10^{-8}	CCl_4	1.3×10^{-10}
CH_4	1.7×10^{-6}	$CFCl_3$	1.4×10^{-10}
H_2	5.3×10^{-7}	CF_2Cl_2	2.4×10^{-10}
CO	see Table A2	CH_3CCl_3	1.1×10^{-10}
N_2O	3.1×10^{-7}	CF_3CCl_3	1.9×10^{-11}
NO_y	see Table A2	CF_3CFCl_2	1.2×10^{-11}
CH_3Cl	6.1×10^{-10}	CH_2FCl	5.4×10^{-11}
CH_2FCl	5.4×10^{-11}	CF_2ClBr	1.7×10^{-12}
$CHFCl_2$	5.2×10^{-11}	CF_3Br	2.0×10^{-12}
CHF_2Cl	5.4×10^{-11}	CH_3Br	see Table A2

Table A2. Mixing Ratios of Long-Lived Species at the Surface in Different Latitude Belts

Latitude	CO	NO_y	CH_3Br
90S–80S	6.39×10^{-8}	1.1×10^{-12}	8.68×10^{-12}
80S–70S	6.39×10^{-8}	1.1×10^{-12}	8.68×10^{-12}
70S–60S	6.40×10^{-8}	1.1×10^{-12}	8.68×10^{-12}
60S–50S	6.48×10^{-8}	1.1×10^{-12}	8.23×10^{-12}
50S–40S	6.62×10^{-8}	2.0×10^{-12}	7.76×10^{-12}
40S–30S	7.02×10^{-8}	2.6×10^{-11}	7.80×10^{-12}
30S–20S	8.03×10^{-8}	2.6×10^{-11}	8.05×10^{-12}
20S–10S	8.99×10^{-8}	9.3×10^{-11}	8.30×10^{-12}
10S–0S	1.01×10^{-7}	1.1×10^{-10}	8.85×10^{-12}
0N–10N	1.02×10^{-7}	3.1×10^{-10}	9.44×10^{-12}
10N–20N	1.02×10^{-7}	3.1×10^{-10}	1.00×10^{-11}
20N–30N	1.07×10^{-7}	4.5×10^{-10}	1.04×10^{-11}
30N–40N	1.18×10^{-7}	4.8×10^{-10}	1.07×10^{-11}
40N–50N	1.26×10^{-7}	1.3×10^{-9}	1.09×10^{-11}
50N–60N	1.29×10^{-7}	1.3×10^{-9}	1.14×10^{-11}
60N–70N	1.25×10^{-7}	1.0×10^{-9}	1.18×10^{-11}
70N–80N	1.21×10^{-7}	1.1×10^{-9}	1.21×10^{-11}
80N–90N	1.20×10^{-7}	2.3×10^{-10}	1.21×10^{-11}

$BrONO_2$, HBr, BrCl, CH_3Br and halons), and the fluorine group (F, FO, FO_2, FNO, FNO_3, COF_2, HF and CFCs). Water vapor is fixed to climatological values in the troposphere and to UARS values in the stratosphere. The numerical method used for solving (A1) in the model is that of *Prather* [1986]. The advantage of this numerical scheme, based on the conservation of second order moments, is that it has almost no numerical diffusion. Hence it is particularly suited for simulating chemical tracers with strong spatial gradients [*Shia et al.*, 1990].

[48] A substantial portion of the photolysis of N_2O in the stratosphere occurs in the Schumann-Runge Bands (SRB) of O_2 (175–205 nm), where the band structure of the absorption spectrum has to be taken into account. The SRB of O_2 is also the primary spectral region in which other molecules such as H_2O, NO, HNO_3, and many CFCs photolyze in the stratosphere. To account for transmission in the SRB, we use the parameterization of *Allen and Frederick* [1982] derived from line-by-line radiative transfer calculations. We will briefly describe three model runs to demonstrate how the model simulates the stratosphere-troposphere exchange and the ozone layer.

[49] Simulations of CO_2 and SF_6 and comparisons with observations provide validation of the transport fields used in the 2-D model. CO_2 is released at the surface, and transported to the stratosphere, where it has no chemical sink and only a very small source from CH_4 oxidation. The annual increase of ~1.5 ppmv CO_2 per year makes this species particularly useful for calculating the mean age of stratospheric air parcels [*Hall and Plumb*, 1994; *Hall and Waugh*, 1997]. For the lower boundary concentrations, we use the data sets collected by the NOAA CMDL effort. For full description of the data, the reader is referred to http://www.cmdl.noaa.gov/ccg/. Weekly flask measurements are available at 47 remote sites from Alaska to the South Pole. We use the monthly mean data from 1984 to 1997, averaged in 10° latitude boxes. Figure A1 shows the results of the comparison between model (10 S to 10 N) and data from balloon and ER-2 aircraft measurements [*Hall et al.*, 1999]. We used the NCEP-GSFC transport. The model age of air agrees well with the observations in the lower stratosphere, but is 0.5 to 1 year too short in the upper stratosphere. An adjustment is made to increase the transport above 30 km, and the revised results (solid line in Figure A1) are in good agreement with observations.

[50] Like CO_2, SF_6 is released at the surface and has an essentially infinite chemical lifetime in the stratosphere. SF_6 has a nearly constant annual growth rate of 8% per year [e.g., *Geller et al.*, 1997]. Unlike CO_2, it does not have a seasonal cycle or stratospheric sources to complicate the calculation of mean age. The SF_6 model boundary con-

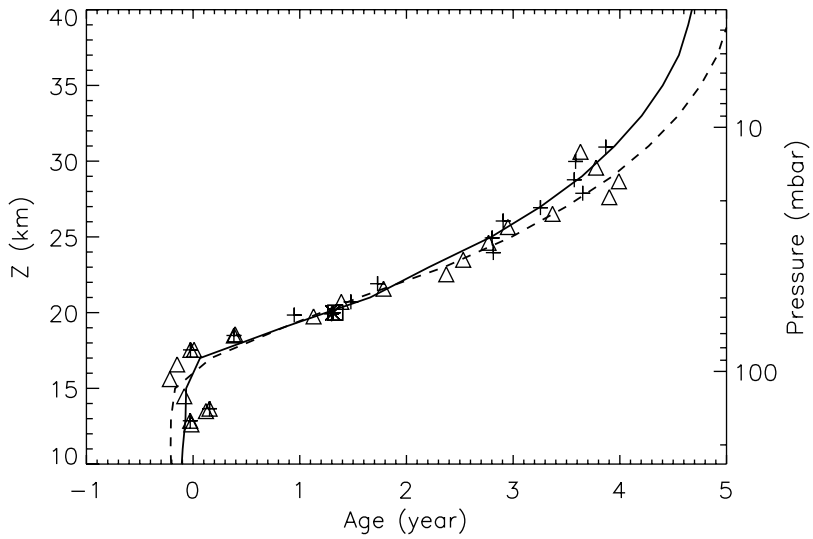

Figure A1. The vertical profile of the yearly averaged age of air over 10 S. to 10 N. derived from the 2-D model simulation of CO_2 (solid line) and SF_6 (dashed line). Also shown are the mean age calculated from OMS balloon measurements of CO_2 (crosses) and SF_6 (triangles) taken during February and November 1997 at 7 S., and ER-2 aircraft measurements of CO_2 (asterisks) and SF_6 (squares) at 20 km averaged over 10 S–10 N during 1992–1997 [*Hall et al.*, 1999].

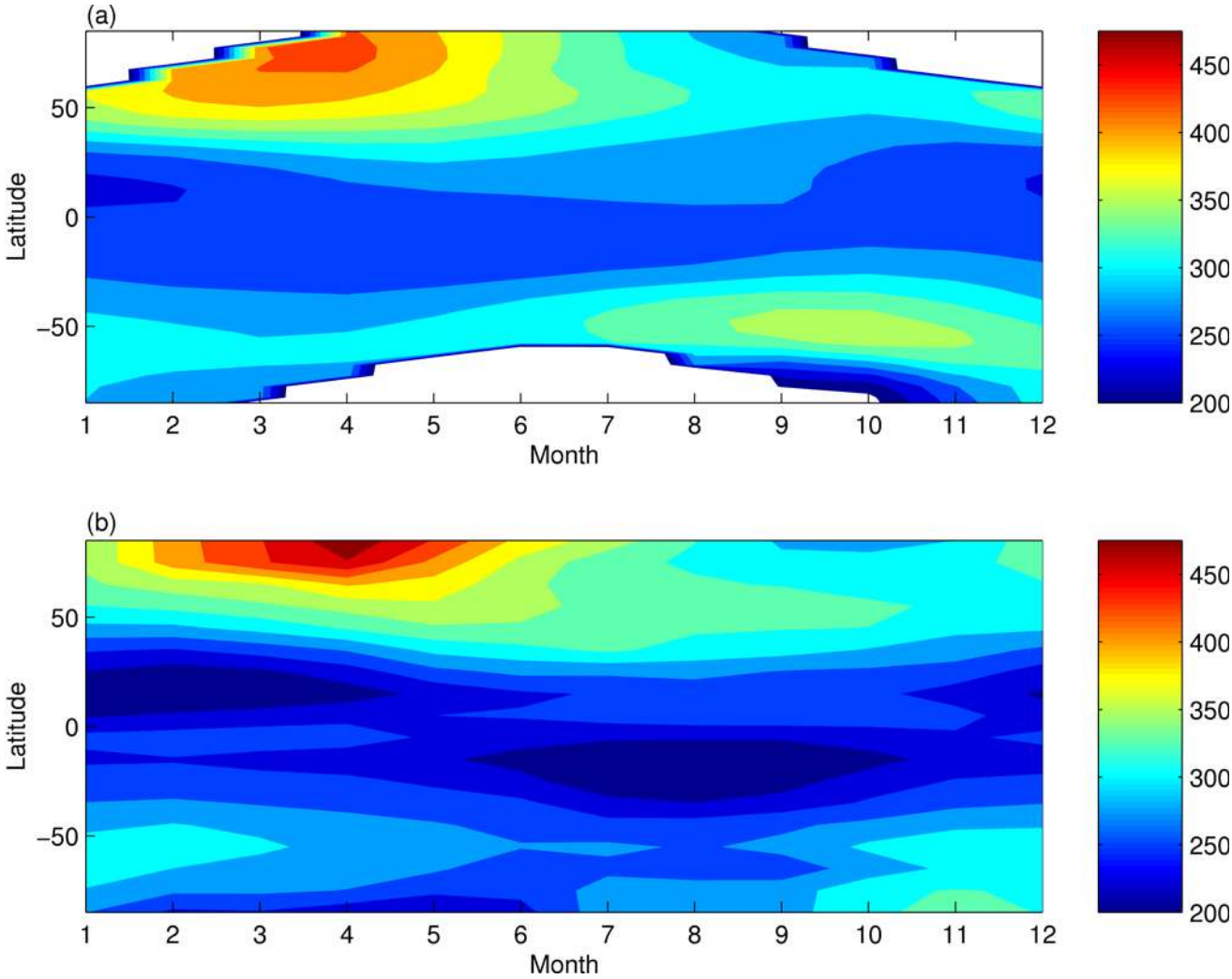

Figure A2. (a) Climatology of ozone column density from TOMS version 7 from 1979 to 2000. The white patches represent areas for which there were no measurements. The data are from *McPeters et al.* [1998]. (b) The latitude-month variation in ozone column density in DU (1 DU = 2.687×10^{16} molecules/cm^2) simulated by our model. The boundary conditions are given in Tables A1 and A2.

ditions are constrained by the measurements of the NOAA's Climate Monitoring and Diagnostic Laboratory (CMDL). We ran the model from 1984 to 1997. The results for the age of air are summarized by the dashed line in Figure A1, and agree well with the observed values. The overall quality of agreement is similar to that for CO_2. The small difference between the model ages of air derived from SF_6 and CO_2 is caused mainly by the seasonal cycle and the somewhat irregular rate of increase of the CMDL CO_2 concentrations used to drive the model at the lower boundary. SF_6 does not have a seasonal cycle.

[51] The main advantage of the 2-D model over the 3-D model appears to be a stable numerical scheme [*Prather*, 1986; *Shia et al.*, 1990] and the ability to fine-tune the transport in the model. This allows our model to reproduce the age of air to within the errors of the measurements, as shown in Figure A1. However, the 3-D model is rigorously based on fundamental principles. Hence there is little room for fine-tuning. In addition, the numerical scheme is less stable [*Eluszkiewicz et al.*, 2002]. For example, *McLinden et al.* [2003] noted, "This latter model is known to have a somewhat stagnant upwelling in the tropical middle stratosphere which leads to unrealistically long N_2O lifetimes and has been traced to GCM numerics." To date, there is only one 3-D model that can satisfactorily reproduce the age of air in the stratosphere by using isentropic coordinates [*Mahowald et al.*, 2002].

[52] We carried out a simulation of stratospheric O_3 using fixed boundary conditions for 1986. After six years, the concentrations are practically indistinguishable from one year to the next. Figure A2 (lower panel) shows the latitude-month variation in ozone column abundance simulated by our model. The units are Dobson Units (1 DU = 2.687×10^{16} molecules/cm^2). The upper panel presents the mean from 1979 to 2000 measured by TOMS and EP TOMS [*McPeters et al.*, 1998] (updates are available at http://toms.gsfc.nasa.gov). The model is able to qualitatively simulate most of the seasonal features, such as the northern spring maximum (>450 DU), as well as the minimum in the tropics (<250 DU). However, the model does not simulate the Antarctic Ozone Hole in the austral spring. The reason is that the loss of O_3 there is caused by heterogeneous

chemistry on the surface of ice particles. The present model does not include heterogeneous chemistry.

Appendix B: Analytic Model for N_2O Isotopic Fractionation

[53] We consider the 1-D diffusion-limited case where the steady state continuity equation, equation (A1) in appendix A, for N_2O is reduced to

$$-e^{\xi}\frac{d}{dz}\left\{e^{-\xi}K_{zz}\frac{d\chi}{dz}\right\}=\frac{Q}{M} \tag{B1}$$

where $\xi = z/H_o$, K_{zz} denotes the vertical eddy diffusivity, Q is the net chemical production and M is the number density of the atmosphere. For simplicity, we assume an isothermal atmosphere with constant scale height H_o. The number density of the atmosphere is given by $M(z) = M_0\exp(-z/H_0)$. The atmosphere consists of two layers, the troposphere ranging from the surface ($z = 0$) to the tropopause ($z = z_1$), and the stratosphere overlying the troposphere. The eddy diffusivity is assumed to be a step function, equal to K_o and K_1 in the troposphere and stratosphere, respectively. Assuming, to a good approximation, that there is no source or sink for N_2O in the troposphere, we have $Q = 0$ for $z < z_1$. In the stratosphere, the loss of N_2O by photolysis is approximated by $Q/M = -J\chi$, where J is the photodissociation coefficient.

[54] With these assumptions the continuity equation (B1) in the troposphere is equivalent to

$$\frac{d\phi}{dz}=0 \tag{B2}$$

where the flux is given by

$$\phi(z)=-K_oM(z)\frac{d\chi}{dz}. \tag{B3}$$

From (B2) we have $\phi(z) = \phi_o$ = constant, and solving (B3) we have

$$\chi(z)=\chi_o+\frac{\phi_oH_o}{K_oM_o}\left(1-e^{z/H_o}\right) \tag{B4}$$

where χ_o and M_o refer to the mixing ratio of N_2O and total number density at the surface, respectively. The RHS of (B4) is dominated by the constant term χ_o. The second term contributes at most a few percent near the tropopause.

[55] In the stratosphere, the continuity equation (B1) becomes

$$\frac{d^2\chi}{dz^2}-\frac{1}{H_o}\frac{d\chi}{dz}-\frac{J}{K_1}\chi=0 \tag{B5}$$

Seeking solutions of the type $e^{\lambda z}$ reduces (B5) to a quadratic equation with two roots

$$\lambda_1=\frac{1}{2H_o}\left(-\sqrt{1+\frac{4JH_o^2}{K_1}}+1\right)$$

$$\lambda_2=\frac{1}{2H_o}\left(\sqrt{1+\frac{4JH_o^2}{K_1}}+1\right)$$

Requiring that the mixing ratio be bounded at $z = \infty$ eliminates the second solution, and the physically acceptable solution is

$$\chi(z)=\chi_1e^{-(z-z_1)/h} \tag{B6}$$

where χ_1 is $\chi(z_1)$ from (B4) and

$$\frac{1}{h}=-\lambda_1=\sqrt{\frac{J}{K_1}}\left(\sqrt{1+r}-\sqrt{r}\right) \tag{B7}$$

with $r = \frac{K_1}{4JH_o^2} < 1$. Equation (B6) provides the fundamental relation between the mixing ratio of N_2O in the stratosphere and its photodissociation coefficient. The result appears to have been first derived by *Kaye* [1987]. For later applications to different isotopologues and isotopomers we need the logarithmic derivative of $\frac{1}{h}$

$$\frac{d\ln(1/h)}{d\ln J}=\frac{1}{2}\left(1+\sqrt{\frac{r}{1+r}}\right) \tag{B8}$$

[56] In order to compute the lifetime of a N_2O molecule in the atmosphere, we need to evaluate its column-integrated abundance and column-integrated loss rate. The number density of N_2O in the stratosphere is given by

$$n(z)=M(z)\chi(z)=M_oe^{-z_1/H_0}\chi_1e^{-(z-z_1)/H_1} \tag{B9}$$

$$\frac{1}{H_1}=\frac{1}{h}+\frac{1}{H_o}=\sqrt{\frac{J}{K_1}}\left(\sqrt{1+r}+\sqrt{r}\right) \tag{B10}$$

[57] The flux from the troposphere, ϕ_o, must balance the column integrated loss of N_2O by photolysis in the stratosphere. We have

$$\phi_o=\int_{z_1}^{\infty}J\cdot n(z)dz \tag{B11}$$

Combining (B4), (B9) and (B11), we have

$$\phi_o=\frac{JM_o\chi_oH_1e^{-z_1/H_o}}{1+\frac{JH_oH_1}{K_o}\left(1-e^{-z_1/H_o}\right)} \tag{B12}$$

The lifetime of N_2O is given by

$$\tau=N/\phi_o \tag{B13}$$

where N is the column density of N_2O

$$N=\int_0^{\infty}M(z)\chi(z)dz \tag{B14}$$

N consists of two parts: N_T, the column in the troposphere and N_S, the column in the stratosphere. Carrying out the appropriate integrals, we have

$$N_T=M_o\chi_oH_o\left(1-e^{-z_1/H_o}\right)+\frac{\phi_oH_o^2}{K_o}\left(1-\frac{z_1}{H_o}-e^{-z_1/H_o}\right) \tag{B15}$$

$$N_s=\frac{M_o\chi_oH_1e^{-z_1/Ho}}{1+\frac{JH_oH_1}{K_o}\left(1-e^{-z_1/H_o}\right)} \tag{B16}$$

Therefore we have

$$\tau = \frac{M_o \chi_o H_o}{\phi_o}\left(1 - e^{-z_1/H_o}\right) + \frac{H_o^2}{K_o}\left(1 - \frac{z_1}{H_o} - e^{-z_1/H_o}\right) + \frac{1}{J} \tag{B17}$$

Note that the first term on the RHS of (B17) dominates. For applications to isotopologues and isotopomers we need the logarithmic derivative of τ

$$\frac{\partial \ln \tau}{\partial \ln J} \approx -\frac{1}{2}\left(1 + \sqrt{\frac{r}{1+r}}\right) \tag{B18}$$

We may now apply the theory to the isotopic fractionation of N_2O. Let A be the abundant isotopologue and B be one of the less abundant isotopologue. From (B6) we have

$$\chi_A(z) = \chi_{1A} e^{-(z-z_1)/h_A} = \chi_{oA} e^{-(z-z_1)/h_A} \tag{B19}$$

where χ_A, $\chi_{1A} \equiv \chi_{oA}$ refer to species A and h_A is the same as h in (B7) with J_A replacing J. Let F be the fraction of residual N_2O in the stratosphere (relative to its concentration in the troposphere)

$$f(z) = \frac{\chi_A(z)}{\chi_{oA}} = e^{-(z-z_1)/h_A} \tag{B20}$$

Applying the same formulas to isotopologue B we have

$$\chi_B(z) \approx \chi_{oB} e^{-(z-z_1)/h_B} \tag{B21}$$

where χ_B, χ_{oB}, and h_B refer to species B. The ratio between the photolysis rate coefficients for isotopologues A and B is given by

$$\alpha = \frac{J_B}{J_A} \tag{B22}$$

Taking the ratio between equations (B19) and (B21), we have

$$\frac{\chi_B(z)}{\chi_A(z)} = \frac{\chi_{oB}}{\chi_{oA}} e^{-(z-z_1)\left(\frac{1}{h_B} - \frac{1}{h_A}\right)} \tag{B23}$$

It is convenient to compare the isotopic ratio χ_B/χ_A to a standard ratio $(\chi_B/\chi_A)_s$ and define the isotopic fractionation δ (in per mil) by

$$\delta = \left[\left(\frac{\chi_B}{\chi_A}\right) \Big/ \left(\frac{\chi_B}{\chi_A}\right)_S - 1\right] \times 1000 \tag{B24}$$

Dividing (B23) by $\left(\frac{\chi_B}{\chi_A}\right)_s$ and taking the logarithm of both sides, we obtain the approximate relation

$$\delta(z) \approx \delta_o + \varepsilon \ln f(z) \tag{B25}$$

where δ_o is $\delta(z = 0)$ and

$$\varepsilon = \frac{h_A}{h_B} - 1 \approx (\alpha - 1)\frac{d \ln \frac{1}{h}}{d \ln J} \tag{B26}$$

This expression for ε may be simplified using (B8) and we have for ε (in per mil)

$$\varepsilon = \frac{1}{2}(\alpha - 1)\left(1 + \sqrt{\frac{r}{1+r}}\right) \times 1000 \tag{B27}$$

$$\varepsilon_i = (\alpha_i - 1)E \tag{B28a}$$

$$E = \frac{1}{2}\left(1 + \sqrt{\frac{r}{1+r}}\right) \tag{B28b}$$

Special cases of (B28) with E = 1 and 0.5, have been obtained by *Rahn and Wahlen* [1997] and *Rahn et al.* [1998], respectively. The first limit obtains for $r \gg 1$, in a situation where transport is very rapid compared to chemical removal. Therefore the effect of transport on ε can be ignored. The second limit corresponds to the case of very slow transport as compared to chemical removal. In this case ε is only to half of its value as in the first case. Our estimate for ε lies between the extreme values first derived by *Rahn and Wahlen* [1997] and *Rahn et al.* [1998]. Using representative values for the atmosphere, $K_1 = 3 \times 10^4$ cm^2 s^{-1}, $J = 4 \times 10^{-8}$ s^{-1}, and H = 7 km, we estimate $r = 0.38$ and E = 0.76. This results in a difference of about 25% between our results for the value of ε and that from previous studies.

[58] For laboratory studies, transport can be assumed to be very rapid in the experimental apparatus, i.e., E = 1. *Röckmann et al.* [2001] report their enrichments as positive numbers and in both their observational and laboratory studies, since they define $\epsilon = (1/\alpha) - 1$. However, it should be noted that this definition of ϵ is inconsistent with their definition of δ, which they define exactly as it is defined in this paper. For consistency, their observational enrichments have been changed to negative values of the same magnitude in Tables 2–4.

[59] Let τ_A and τ_B be the mean lifetimes of isotopologues A and B averaged over the atmosphere, derived using (B17) for A and B. We can derive the approximate expression for $\delta\tau$ (in per mil)

$$\delta\tau = \frac{\tau_B}{\tau_A} - 1 = (\alpha - 1)\frac{d \ln \tau}{d \ln J} \tag{B29}$$

From (B18) and (B27) we can simplify (B29) to

$$\delta\tau = -\varepsilon = -\frac{1}{2}(\alpha - 1)\left(1 + \sqrt{\frac{r}{(r+r)}}\right) \times 1000 \tag{B30}$$

Expressions (B25), (B27) and (B30) provides simple but highly accurate relations between the isotopic fraction $\delta(z)$, the ratio between dissociation coefficients α and the fractional difference in average lifetimes $\delta\tau$. These approximations are accurate to better than 1% in the context of the 1-D model.

Appendix C: Nonstandard Chemistry for N_2O Production

[60] *Zipf and Prasad* [1998] presented laboratory data in support of a nonstandard source of N_2O in the atmosphere. The reaction is initiated by the formation of an excited intermediate O_3^{N2O} via

$$O + O_2 + M \rightarrow O_3^{N2O} + M \tag{C1}$$

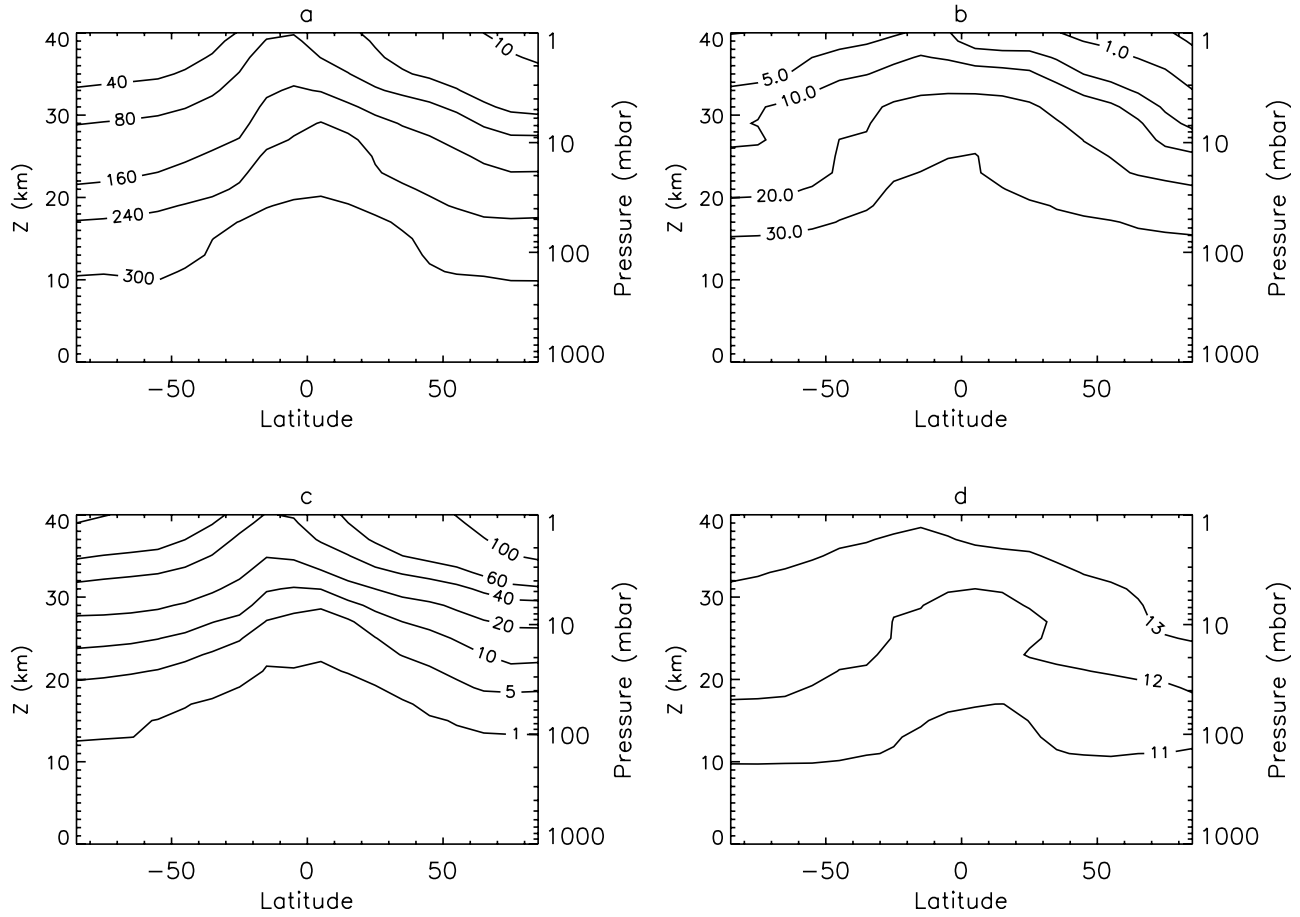

Figure C1. (a) Mixing ratio of N_2O in ppbv as a function of altitude and latitude in January computed by the standard model. (b) Increase in mixing ratio of N_2O in ppbv when a new source of N_2O is added to the reference case in Figure C1a. (c) Same as in Figure C1a for δ_{448}. (d) Same as in C1b for δ_{448}.

followed by

$$O_3^{N2O} + N_2 \rightarrow O_2 + N_2O \quad \text{(C2)}$$

The net result is equivalent to

$$O + O_2 + N_2 \rightarrow O_2 + N_2O \quad \text{(C3)}$$

The authors estimated a quantum yield

$$Q_{ZP} = 4 \times 10^{-5} \times [p/(p + a)] \quad \text{(C4)}$$

where p is the atmospheric pressure in mbar and a = 380 mbar. As we will show, the proposed quantum yield strongly violates the observational constraints, and therefore we reduce it by a factor $\beta < 1$

$$Q = Q_{ZP} \times \beta \quad \text{(C5)}$$

The authors did not report the quantum yield for the (448) isotopologue. However, it is most likely that reaction (C1) favors the heavy ozone. Therefore we expect the quantum yield for (448) to be larger than that for (446)

$$Q(448) = Q(446)[1 + \delta/1000] \quad \text{(C6)}$$

We adopt the value $\delta = 100$ by analogy with the enrichment for heavy O_3 [*Mauersberger et al.*, 1993].

[61] We carried out several model runs with β between 0 and 0.1. Figure C1a shows the mixing ratio of N_2O in ppbv in the atmosphere for January as computed by our standard model. Figure C1b shows the increase in the mixing ratios of N_2O due to the inclusion of the new source with $\beta = 0.03$. This choice of the value for β corresponds to a new N_2O source of 1.53 Tg N yr^{-1}. The increase in N_2O mixing ratio is about 10% through the atmosphere. Figure C1c presents the isotopic fractionation of the (448) isotopologue in the standard model for January. Figure C1d presents the increase in fractionation due to the new source. The values for δ_{448} increase by more than 10‰ throughout the atmosphere. Thus the new source has a very different pattern for δ_{448} than that caused by photolysis. The reason is that the bulk of reaction (RC3) occurs below 20 km, while the bulk of photolysis occurs above 25 km, as shown in Figure 7.

[62] **Acknowledgments.** We thank D. Griffith for revised data, E. Fleming for sending us his stream functions, T. Rahn, M. Gerstell and S. Olsen for helpful comments, and R. Li for compiling the references. We thank two anonymous referees for painstakingly pointing out a number of inaccuracies in the early versions of this paper and for suggesting significant improvements of the paper. We especially thank the editor D. Toohey for his patience in guiding this paper through its reviews. This work was supported in part by an NSF grant ATM-9903790. The updating of the Caltech/JPL 2-D model was supported by NASA grant NAG1-1806.

References

Allen, M., and J. E. Frederick (1982), Effective photo-dissociation cross-sections for molecular-oxygen and nitric-oxide in the schumann-runge bands, *J. Atmos. Sci.*, *39*, 2066–2075.

Allen, M., et al. (1981), Vertical transport and photochemistry in the terrestrial mesosphere and lower thermosphere (50–120 km), *J. Geophys. Res.*, *86*, 3617–3627.

Blake, G. A., M.-C. Liang, C. G. Morgan, and Y. L. Yung (2003), A Born-Oppenheimer photolysis model of N_2O fractionation, *Geophys. Res. Lett.*, *30*(12), 1656, doi:10.1029/2003GL016932.

Brown, M. (1993), Deduction of emissions of source gases using an objective inversion algorithm and a chemical-transport model, *J. Geophys. Res.*, *98*, 12,639–12,660.

Cicerone, R. J. (1989), Analysis of sources and sinks of atmospheric nitrous oxide (N_2O), *J. Geophys. Res.*, *94*, 18,265–18,271.

DeMore, W. B., et al. (1997), Chemical kinetics and photochemical data for use in stratospheric modeling, *Evaluation 12, Pub. 97-4*, Jet Propulsion Lab., Pasadena, Calif.

Eluszkiewicz, J., et al. (1996), Residual circulation in the stratosphere and lower mesosphere as diagnosed from Microwave Limb Sounder data, *J. Atmos. Sci.*, *53*, 217–240.

Eluszkiewicz, J., et al. (2002), Sensitivity of age-of-air calculations to the choice of advection scheme, *J. Atmos. Sci.*, *57*(19), 3185–3201.

Fleming, E. L., C. H. Jackman, J. E. Rosenfield, and D. B. Considine (2002), Two-dimensional model simulations of the QBO in ozone and tracers in the tropical stratosphere, *J. Geophys. Res.*, *107*(D23), 4665, doi:10.1029/2001JD001146.

Flückiger, J., et al. (1999), Variations in atmospheric N_2O concentration during abrupt climatic changes, *Science*, *285*, 227–230.

Fortuin, J. P. F., and H. Kelder (1998), An ozone climatology based on ozonesonde and satellite measurements, *J. Geophys. Res.*, *103*, 31,709–31,734.

Garcia, R. R., and S. Solomon (1983), A numerical-model of the zonally averaged dynamical and chemical-structure of the middle atmosphere, *J. Geophys. Res.*, *88*, 1379–1400.

Geller, L. S., J. W. Elkins, J. M. Lobert, A. D. Clarke, D. F. Hurst, J. H. Butler, and R. C. Myers (1997), Tropospheric SF_6: Observed latitudinal distribution and trends, derived emissions and interhemispheric exchange time, *Geophys. Res. Lett.*, *24*, 675–678.

Griffith, D., G. Toon, B. Sen, J. Blavier, and R. Toth (2000), Vertical profiles of nitrous oxide isotopomer fractionation measured in the stratosphere, *Geophys. Res. Lett.*, *27*, 2485–2488.

Gunson, M. R., C. B. Farmer, R. H. Norton, R. Zander, C. P. Rinsland, J. H. Shaw, and B.-C. Gao (1990), Measurements of CH_4, N_2O, CO, H_2O, and O_3 in the middle atmosphere by the Atmospheric Trace Molecule Spectroscopy Experiment on Spacelab 3, *J. Geophys. Res.*, *95*, 13,867–13,882.

Hall, T. M., and R. A. Plumb (1994), Age as a diagnostic of stratospheric transport, *J. Geophys. Res.*, *99*, 1059–1070.

Hall, T. M., and D. W. Waugh (1997), Timescales for the stratospheric circulation derived from tracers, *J. Geophys. Res.*, *102*, 8991–9001.

Hall, T., D. Waugh, K. Boering, and R. Plumb (1999), Evaluation of transport in stratospheric models, *J. Geophys. Res.*, *104*, 18,815–18,840.

Houghton, J. T., G. J. Jenkins, and J. J. Ephraums (Eds.) (1990), *Climate Change: The IPCC Scientific Assessment*, Cambridge Univ. Press, New York.

Houghton, J. T., L. G. Meira Filho, B. A. Callander, N. Harris, A. Kattenberg, and K. Maksell (Eds.) (1996), *Climate Change: The Science of Climate Change*, Cambridge Univ. Press, New York.

Houghton, J. T., Y. Ding, D. J. Griggs, M. Noguer, P. J. van der Linden, X. Dai, K. Maskell, and C. A. Johnson (Eds.) (2001), *Climate Change 2001: The Scientific Basis*, Cambridge Univ. Press, New York.

Johnson, M. S., et al. (2001), Photolysis of nitrous oxide isotopomers studied by time-dependent Hermite propagation, *J. Phys. Chem. A.*, *105*, 8672–8680.

Johnston, J. C., et al. (1995), Measurements of multi-oxygen isotopic (δ-^{18}O and δ-^{17}O) Fractionation factors in the stratospheric sink reactions of nitrous oxide, *J. Geophys. Res.*, *100*, 16,801–16,804.

Kaiser, J., T. Rockmann, and C. A. M. Brenninkmeijer (2002a), Temperature dependence of isotope fractionation in N2O photolysis, *Phys. Chem. Chem. Phys*, *4*, 4420–4430.

Kaiser, J., C. A. M. Brenninkmeijer, and T. Röckmann (2002b), Intramolecular ^{15}N and ^{18}O fractionation in the reaction of N_2O with $O(^1D)$ and its implications for the stratospheric N_2O isotope signature, *J. Geophys. Res.*, *107*(D14), 4214, doi:10.1029/2001JD001506.

Kaiser, J., et al. (2003), Wavelength dependence of isotope fractionation in N_2O photolysis, *Atmos. Chem. Phys.*, *3*, 303–313.

Kaye, J. A. (1987), Mechanisms and observations for isotope fractionation of molecular-species in planetary-atmospheres, *Rev. Geophys.*, *25*, 1609–1658.

Khalil, M. A. K., and R. A. Rasmussen (1992), The global sources of nitrous oxide, *J. Geophys. Res.*, *97*, 14,651–14,660.

Khalil, M. A. K., and R. A. Rasmussen (1995), The changing composition of the earth's atmosphere, *Composition, Chemistry and Climate of the Atmosphere*, edited by H. B. Singh, pp. 50–87, Van Nostrand Reinhold, New York.

Kim, K.-R., and H. Craig (1990), Two isotope characterization of N_2O in the Pacific Ocean and constrains on its origin in deep water, *Nature*, *347*, 58–61.

Kim, K.-R., and H. Craig (1993), ^{15}N and ^{18}O characteristics of nitrous oxide-a global perspective, *Science*, *262*, 1855–1857.

Ko, M. K. W., et al. (1985), A zonal mean model of stratospheric tracer transport in isentropic coordinates-numerical simulations for nitrous oxide and nitric acid, *J. Geophys. Res.*, *90*, 2313–2329.

Leuenberger, M., and U. Siegenthaler (1992), Ice-age atmospheric concentration of nitrous oxide from an Antarctic ice core, *Nature*, *360*, 449–451.

Logan, J. A., et al. (1978), Atmospheric chemistry: Response to human influence, *Philos. Trans. R. Soc. London*, *290*, 187–234.

Mahowald, N. M., R. A. Plumb, P. J. Rasch, J. del Corral, F. Sassi, and W. Heres (2002), Stratospheric transport in a three-dimensional isentropic coordinate model, *J. Geophys. Res.*, *107*(D15), 4254, doi:10.1029/2001JD001313.

Mauersberger, K., J. Morton, B. Schueler, J. Stehr, and S. Anderson (1993), Multiisotope study of ozone: Implications for the heavy ozone anomaly, *Geophys. Res. Lett.*, *20*(11), 1031–1034.

McElroy, M. B., and D. B. A. Jones (1996), Evidence for an additional source of atmospheric N_2O, *Global Biogeochem. Cycles*, *10*, 651–659.

McElroy, M. B., et al. (1977), The nitrogen cycle: Perturbations due to man and their impact on atmospheric N_2O and O_3, *Proc. R. Soc. London*, *277*, 159–181.

McLinden, C. A., M. J. Prather, and M. S. Johnson (2003), Global modeling of the isotopic analogues of N_2O: Stratospheric distributions, budgets, and the ^{17}O-^{18}O mass-independent anomaly, *J. Geophys. Res.*, *108*(D8), 4233, doi:10.1029/2002JD002560.

McPeters, R. D., et al. (1998), Earth Probe Total Ozone Mapping Spectrometer (TOMS) Data Product User's Guide, *NASA Tech. Publ., 206895*, 67 pp.

Mérienne, M., et al. (1990), Temperature effect on the ultraviolet absorption of CFC_{l3}, CF_2C_{l2}, and N_2O, *Planet. Space Sci.*, *38*, 617–625.

Minschwaner, K., R. Salawitch, and M. McElroy (1993), Absorption of solar radiation by O_2: Implications for O_3 and lifetimes of N_2O, $CFCl_3$, and CF_2Cl_2, *J. Geophys. Res.*, *98*(D6), 10,543–10,561.

Morgan, C. G., Y. L. Yung, M. A. Allen, G. A. Blake, and M. C. Liang (2002), Isotopic fractionation of atmospheric nitrous oxide, *Eos Trans. AGU*, *83*(19), Spring Meet. Suppl., Abstract B22D-01.

Nevison, C., and E. Holland (1997), A reexamination of the impact of anthropogenically fixed nitrogen on atmospheric N_2O and the stratospheric O_3 layer, *Geophys. Res. Lett.*, *102*, 25,519–25,536.

Nightingale, R. W., et al. (1993), CLAES N_2O and CH_4 Tracer Gas Comparisons with Correlative Measurements in the Stratosphere, *Eos Trans. AGU*, *74*(43), Fall Meet. Suppl., F112.

Olsen, S., C. McLinden, and M. Prather (2001), Stratospheric N_2O-NO_y system: Testing uncertainties in a three-dimensional framework, *J. Geophys. Res.*, *106*(D22), 28,771–28,784.

O'Neil, J. R., (1986), Terminology and Standards, in *Stable Isotopes in High Temperature Geological Processes*, *Rev. in Mineral.*, vol. 16, edited by J. W. Valley, H. P. Taylor, and J. R. O'Neil, pp. 561–570, Mineral. Soc. of Am., Washington, D. C.

Prasad, S. S. (1994), Natural atmospheric sources and sinks of nitrous oxide: 1. An evaluation based on 10 laboratory experiments, *J. Geophys. Res.*, *99*, 5285–5294.

Prasad, S. S. (1997), Potential atmospheric sources and sinks of nitrous oxides: 2. Possibilities from excited O_2, "embryonic: O_3, and optically pumped excited O_3, *J. Geophys. Res.*, *102*, 21,527–21,536.

Prasad, S. S. (1998), Potential new atmospheric sources and sinks of odd nitrogen: Sources involving the excited O_2, and the N_2O center dot O_3 species, *Geophys. Res. Lett.*, *25*, 2173–2176.

Prather, M. J. (1986), Numerical advection by conservation of 2nd-order moment, *J. Geophys. Res.*, *91*, 6671–6681.

Prinn, R. G., et al. (2000), A history of chemically and radiatively important gases in air deduced from ALE/GAGE/AGAGE, *J. Geophys. Res.*, *105*, 17,751–17,792.

Proffitt, M., S. Solomon, and M. Lowenstein (1992), Comparison of 2-D model simulations of ozone and nitrous oxide at high latitudes with stratospheric measurements, *J. Geophys. Res.*, *97*, 939–944.

Rahn, T., and M. Wahlen (1997), Stable isotope enrichment in stratospheric nitrous oxide, *Science*, *278*, 1776–1778.

Rahn, T., and M. Wahlen (2000), A reassessment of the global isotopic budget of atmospheric nitrous oxide, *Global Biogeochem. Cycles*, *14*, 537–543.

Rahn, T., H. Zhang, M. Wahlen, and G. Blake (1998), Stable isotope fractionation during ultraviolet photolysis of N_2O, *Geophys. Res. Lett.*, *25*, 4489–4492.

Randel, W. J., and F. Wu (1999), A stratospheric ozone trends data set for global modeling studies, *Geophys. Res. Lett.*, *26*, 3089–3092.

Röckmann, T., C. A. M. Brenninkmeijer, M. Wollenhaupt, J. N. Crowley, and P. J. Crutzen (2000), Measurement of the isotopic fractionation of $^{15}N^{14}N^{16}O$, $^{14}N^{15}N^{16}O$, and $^{14}N^{14}N^{18}O$ in the UV photolysis of nitrous oxide, *Geophys. Res. Lett.*, *27*, 1399–1402.

Röckmann, T., J. Kaiser, C. A. M. Brenninkmeijer, J. N. Crowley, R. Borchers, W. A. Brand, and P. J. Crutzen (2001), Isotopic enrichment of nitrous oxide ($^{15}N^{14}N^{16}O$, $^{14}N^{15}N^{16}O$, and $^{14}N^{14}N^{18}O$) in the stratosphere and in the laboratory, *J. Geophys. Res.*, *106*, 10,403–10,410.

Röckmann, T., et al. (2003), The isotopic fingerprint of the preindustrial and the anthropogenic, *Atmos. Chem. Phys.*, *3*, 315–323.

Selwyn, G., J. Podolske, and H. S. Johnston (1977), Nitrous oxide ultraviolet absorption spectrum at stratospheric temperatures, *Geophys. Res. Lett.*, *4*, 427–430.

Shia, R., Y. Yung, M. Allen, R. Zurek, and D. Crisp (1989), Sensitivity study of advection and diffusion coefficients in a two-dimensional stratospheric model using excess carbon 14 data, *J. Geophys. Res.*, *94*, 18,467–18,484.

Shia, R. L., Y. L. Ha, J. S. Wen, and Y. L. Yung (1990), Two-dimensional atmospheric transport and chemistry model-numerical experiments with a new advection algorithm, *J. Geophys. Res.*, *95*, 7467–7483.

Stein, L. Y., and Y. L. Yung (2003), Production, isotopic composition, and atmospheric fate of biologically produced nitrous oxide, *Annu. Rev. Earth Plant. Sci.*, *31*, 329–356.

Summers, M. E., D. E. Siskind, J. T. Bacmeister, and S. Zasadil (1997), Seasonal variation of middle atmospheric CH_4 and H_2O with a new chemical-dynamical model, *J. Geophys. Res.*, *102*, 3503–3526.

Toyoda, S., N. Yoshida, and T. Urabe (2000), Fractionation of N_2O isotopomers in the stratosphere, *J. Geophys. Res.*, *106*, 75152001.

Tung, K. K. (1982), On the two-dimensional transport of stratospheric trace gases in the isentropic coordinates, *J. Atmos. Sci.*, *39*, 2330–2355.

Turatti, F., D. Griffith, S. Wilson, M. Esler, T. Rahn, H. Zhang, and G. Blake (2000), Positionally dependent 15N fractionation factors in the UV photolysis of N_2O determined by high resolution FTIR spectroscopy, *Geophys. Res. Lett.*, *27*, 2489–2492.

Wang, W. C., et al. (1976), Greenhouse effects due to man-made perturbations of trace gases, *Science*, *194*, 685–690.

Weiss, R. F. (1981), The temporal and spatial distribution of tropospheric nitrous oxide, *J. Geophys. Res.*, *86*, 7185–7195.

Wennberg, P. O., et al. (1994), Removal of stratospheric O_3 by radicals-in-situ measurements of OH, HO_2, NO, NO_2, ClO, and BrO, *Science*, *266*, 398–404.

Yoshida, N., and S. Toyoda (2000), Constraining the atmospheric N_2O budget from intramolecular site preference in N_2O isotopomers, *Nature*, *405*, 330–334.

Yoshino, K., D. E. Freeman, and W. H. Parkinson (1984), High resolution absorption cross-section measurements of N_2O at 295–299 K, *Planet. Space Sci.*, *32*, 1219–1222.

Yung, Y. L. (2002), The mean isotopic composition of nitrous oxide inferred from atmospheric modeling, *Eos Trans. AGU*, *83*(47), Fall Meet. Suppl., Abstract B71A-0700.

Yung, Y. L., and C. E. Miller (1977), Isotopic fractionation of stratospheric nitrous oxide, *Science*, *278*, 1778–1780.

Yung, Y. L., W. C. Wang, and A. A. Lacis (1976), Greenhouse effect due to atmospheric nitrous oxide, *Geophys. Res. Lett.*, *3*, 619–621.

Yung, Y. L., et al. (1996), Dust: A diagnostic of the hydrological cycle during the Last Glacial Maximum, *Science*, *271*, 962–963.

Zander, R., D. H. Ehhalt, C. P. Rinsland, U. Schmidt, E. Mahieu, J. Rudolph, P. Demoulin, G. Roland, L. Delbouille, and A. J. Sauval (1994), Secular trend and seasonal variability of the column abundance of N_2O above the Jungfraujoch station determined from IR solar spectra, *J. Geophys. Res.*, *99*, 16,745–16,756.

Zipf, E. C., and S. S. Prasad (1998), Experimental evidence that excited ozone is a source of nitrous oxide, *Geophys. Res. Lett.*, *25*, 4333–4336.

Zhang, H., P. O. Wennberg, V. H. Wu, and A. G. Blake (2000), Fractionation of $^{14}N^{15}N^{16}O$ and $^{15}N^{14}N^{16}O$ during photolysis at 213 nm, *Geophys. Res. Lett.*, *27*, 2481–2484.

M. Allen, G. A. Blake, M. C. Liang, R. L. Shia, and Y. L. Yung, Division of Geological and Planetary Sciences, California Institute of Technology, Mail Stop 150-21, Pasadena, CA 91125, USA. (yly@gps.caltech.edu)

C. G. Morgan, SRI International Molecular Physics Laboratory, 333 Ravenswood Ave., Menlo Park, CA 94025, USA.